UC San Diego
UC San Diego Electronic Theses and Dissertations

Title

Investigating the use of wing sweep for pitch control of a small unmanned air vehicle

Permalink

https://escholarship.org/uc/item/6x45r64k

Author

Wright, Kim

Publication Date

2011

Peer reviewed|Thesis/dissertation

UNIVERSITY OF CALIFORNIA, SAN DIEGO

Investigating the Use of Wing Sweep for Pitch Control of a Small Unmanned Air Vehicle

A thesis submitted in partial satisfaction of the

requirements for the degree

Master of Science

in

Engineering Sciences (Aerospace Engineering)

by

Kim Wright

Committee in charge:

Professor Thomas R. Bewley, Chair
Professor Hyonny Kim
Professor John Kosmatka

2011

The thesis of Kim Wright is approved and it is acceptable in quality and form for publication on microfilm and electronically:

_____

_____

_____
Chair

University of California, San Diego

2011

TABLE OF CONTENTS

LIST OF ABBREVIATIONS

AOA	Angle Of Attack
AMA	Academy of Model Aeronautics
ATV	Adjustable Travel Volume
CA	Cyanoacrylate
CFD	Computational Fluid Dynamics
CG	Center of Gravity
AR	Aspect Ratio
ESC	Electronic Speed Controller
IMU	Inertial Measurement Unit
JSF	Joint Strike Fighter
MAV	Micro Air Vehicle
MATLAB	Matrix Laboratory (By Mathworks, Inc.)
NASA	National Aeronautics and Space Administration
NP	Neutral Point
PWM	Pulse Width Modulation
RC	Remote Controlled
SM	Static Margin
UAV	Unmanned Air Vehicle
VTOL	Vertical Takeoff Or Landing
WL	Wing Loading

LIST OF SYMBOLS

α Angle of attack

$C_{m,tot}$ Total pitching moment coefficient

Re   Reynold's number

LIST OF FIGURES

LIST OF GRAPHS

LIST OF TABLES

ABSTRACT OF THE THESIS

Investigating the Use of Wing Sweep for Pitch Control of a Small Unmanned Air Vehicle

By

Kim Wright

Master of Science in Engineering Sciences (Aerospace Engineering)

University of California San Diego, 2011

Professor Thomas R. Bewley, Chair

Small Unmanned Air Vehicles (UAVs) are versatile tools with both civilian and military applications. Fixed wing UAVs require forward airspeed to remain airborne, usually resulting in constant energy expenditure to loiter over targets. A UAV capable of perching could reduce energy expenditure by settling on a site near the target, thus increasing mission duration. Avian perching techniques were observed to build a hypothesis for the biological control techniques employed during the landing maneuver. Variation of wing sweep for pitch control was identified as a contributing control method, and selected for study. A biologically-inspired aircraft was designed with variable wing sweep, and modeled using a combination of MATLAB and Athena Vortex Lattice (AVL) to predict pitching response due to wing sweep. A small remote controlled prototype was built with variable wing sweep in addition to standard flight control surfaces. An onboard microcontroller and inertia measurement unit (IMU) were used to record pitch and wing sweep data during flight. Pitch response to wing sweep was observed, and a proportional integral derivative (PID) control system was designed to successfully use wing sweep for closed loop pitch control.

Chapter 1

Introduction

In this chapter we introduce the current usage of small unmanned air vehicles (UAVs), and discuss the motivation for perching. We will also explore various methods of perching and how these methods have been implemented. This will be followed by a discussion of why we are interested in biologically-inspired perching, and how this relates to the immediate goal of using wing sweep for pitch control.

1.1 Current Use of Unmanned Air Vehicles

Unmanned air vehicles (UAVs) can be used for a variety of military and civilian missions. Advances in sensor, computing, and communications technologies have fueled the development of UAVs, permitting them to grow rapidly from a science fiction concept to widespread use. These aircraft are made in a range of sizes from hummingbird-sized micro air vehicles (MAVs) to aircraft the scale of commercial aircraft (see Figure 1.1). Furthermore, UAVs are made in a plethora of configurations depending upon the mission requirement, varying from jet-powered fixed wing aircraft to small electric quadrotors. However, even with such a large degree of variation, a few concepts are desirable for all UAVs: minimize energy expenditure, maximize available mission time, and reduce cost and complexity whenever possible.

Figure 1.1: A military Global Hawk aircraft being maintained by soldiers.

1.1.1 Small UAVs

Small UAVs are becoming popular tools due to their low cost, relatively simple operation, and flexibility. Many small UAVs can be easily carried by soldiers, and fixed wing models are often hand launched (tossed into the air for takeoff) to permit operation regardless of the terrain (see Figure 1.2). Such flexibility permits these aircraft to be used for immediate surveillance of an area, and identification of nearby threats or resources. Similarly, these aircraft can be operated by civilians in rough terrain for search and rescue missions, such as in the case of an earthquake-damaged urban area. In both situations, hand launching can permit the aircraft to be flown without the need for a large smooth takeoff surface. However, landing in such situations generally requires a small area to slide the aircraft onto the ground, preferably a clear patch of grass or sand. Other solutions include nets to catch aircraft midair, or water landing if available. Regardless of this drawback, small fixed wing UAVs are very useful tools with many current and potential mission options.

Figure 1.2: Aerovironment Inc.'s "Raven" UAV [Aerovironment.]

1.1.2 The Surveillance Mission

A common use for small UAVs is for surveillance of an immediate area, and may require the UAV to monitor a specific target for an extended period of time. For fixed wing UAVs, this requires the aircraft to loiter over the target at altitude, expending energy for propulsion (see Figure 1.3). This constant energy drain will significantly limit mission duration. In addition, the aircraft may need to loiter at significant altitudes to reduce risk of detection. If the aircraft must fly at higher altitudes, it could require sophisticated sensor systems to observe the terrestrial target below.
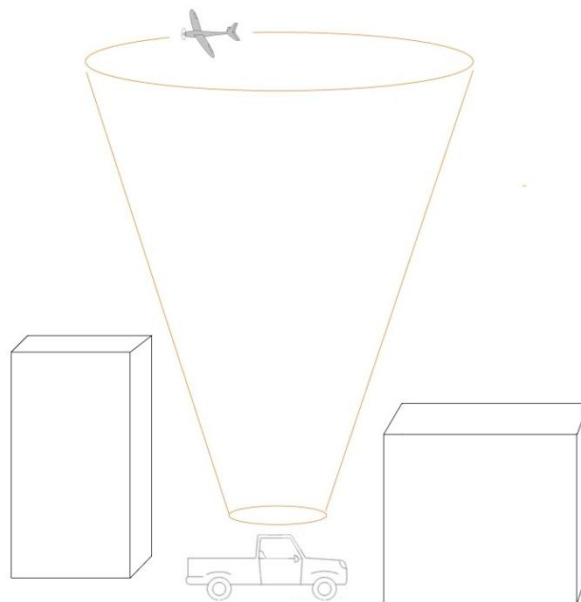
Figure 1.3: UAV loitering over target.

In comparison, a UAV capable of perching (spot landing on a target) on nearby structures (building, poles, etc.) can remain near the target for an extended period of time (see Figure 1.4). The aircraft does not have to expend energy to stay aloft, allowing it to conserve energy by using power only for sensor and communications systems. Because it can observe the target at a much closer range, it can use less sophisticated sensor systems than the UAV loitering at altitude.
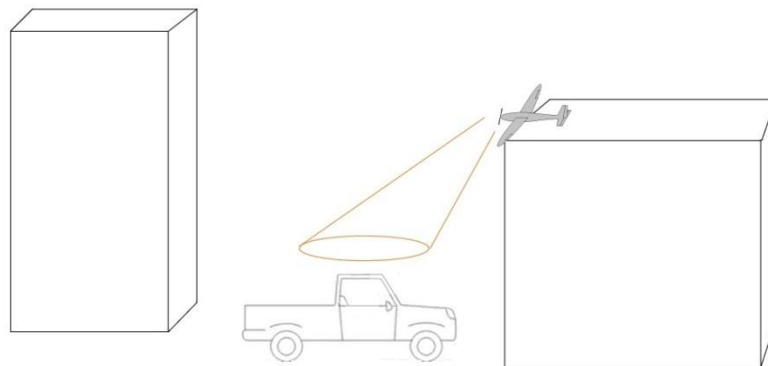
Figure 1.4: UAV perched near target.

1.2   Perching Methods

1.2.1 Current Aircraft Perching Methods

Vertical takeoff and landing (VTOL) is a common occurrence with today's aircraft, as demonstrated by helicopters, the tilt-wing V-22 Osprey (see Figure 1.5), and fixed wing aircraft such as the harrier and joint strike fighter (JSF). In these cases, VTOL is accomplished by relying on powerful engines to provide downward thrust.

Figure 1.5: A military V-22 Osprey tiltrotor aircraft.

A common technique used by remote controlled (RC) aircraft enthusiasts is to 'prop hang' their aircraft (see Figure 1.6). This requires using the aircraft's powerful engine to suspend the aircraft while the pilot grabs it out of the air (or cuts power to drop the plane onto the ground directly below.)

Figure 1.6: Prop-hanging an RC airplane [RegHeath.]

The prop-hanging technique was used by a team of researchers at the Massachusetts Institute of Technology (MIT) to successfully hook the airplane onto a wire using intelligent control [Tedrake 09]. The aircraft was controlled by an off board computer which monitored the aircraft's position relative to the target wire, and used radio communication to control the aircraft's position while prop-hanging. This demonstration certain highlights the potential prop-hanging has for spot landing a small fixed wing UAV on a wire, but scope was limited to aircraft with a power to weight ratio conducive to prop-hanging.

Another maneuver of interest is the 'timed stall' perching approach. This maneuver involves stalling a small fixed wing airplane at the moment it approaches its target landing site. Researchers at Stanford University have successfully used this method to intelligently land their small fixed wing aircraft on the sides of buildings [Desbiens]. The aircraft is flown towards a wall, and a sensor onboard detects the distance between the airplane and the wall. The elevator is then used to induce a rapid pitch up moments before hitting the wall. The airplane pitches up, stalls, and slides against the wall. The landing gear was modified to grab rough surfaces, allowing the plane to stick to the wall. This impressive project demonstrates the effectiveness of the timed stall approach to spot-landing a small, lightweight UAV on a vertical surface.

1.2.2   Perching in Nature

By far the world's most popular perching method is achieved through a combination of wing morphing and flapping. Insects, birds, and bats all display the ability to perch on a target by manipulating their wings during landing approach. The exact method used will vary between species and environment, but all species are capable of landing maneuvers unmatched by manmade machines. Evolution has driven the optimization of each species in their environment, demanding that the animal be capable of spot landing in order to survive. As a result, nature has provided thousands of efficient spot landing models for our analysis and consideration.

Chapter 2

The Avian Perching Problem

This chapter will discuss the logic behind comparing small UAVs to birds, and examine avian flow control techniques and how these can be applied to UAVs. A hypothesis for the avian landing technique will be presented, leading to how the use of wing sweep for pitch control was selected for immediate study.

2.1 Comparing Small UAVs to Birds

2.1.1 Environmental Similarity

Small UAVs and birds often operate in similar environments, with similar goals. Consider the case of a falcon living in an urban area: the animal tends to fly near the ground to search for prey, requiring the ability to maneuver between buildings. In addition, the bird will perch on structures to nest, rest, eat, or scan for prey (see Figure 2.1). The ability to fly near and around buildings is ideal for a small UAV surveying an urban environment, and the capability to perch would permit that UAV to conserve energy while monitoring the target area. Therefore, the avian solution to maneuvering and perching is applicable to the typical mission of a small UAV.

Figure 2.1: A falcon rests on a chimney, displaying urban flexibility [Goldner.]

2.1.2 Reynold's Number Comparison

In order to make an appropriate comparison between a small UAV and a bird, it is important to make sure that both models are operating at the same Reynold's number (Re). This dimensionless parameter quantifies the relationship between inertial effects and viscosity in a fluid flow as described by (2.1), and varies according to the scale of fluid flow. This parameter is fundamental in predicting how an object will behave in a given fluid flow, and must be taken into consideration when comparing two aerodynamic objects.

$$Re = \frac{\rho V L}{\mu} \tag{2.1}$$

When considering the flight of birds and small UAVs, the flow density (ρ) and viscosity (μ) will be the same for both models. Furthermore, both tend to operate at similar speeds (V), often with cruising speeds between 10 and 20 mph. The wing chord is used for the length parameter (L) for both the bid and the small UAV. Because both models have similar chord lengths, it is therefore reasonable to expect that a small UAV can be designed to mimic the maneuvers similarly-sized birds display.

2.2 Avian Flow Control Methods

2.2.1 Avian Wing Morphing Capabilities

Birds have an array of flow control methods available to them, allowing them to perform complex aerial maneuvers (see Figure 2.2). Their wing joints are analogous to our own shoulder and elbow joints, permitting similar degrees of freedom. This allows a variety of wing morphing possibilities:

- Lift and lower wing at shoulder (propulsive flapping and dihedral angle control)
- Wing twist at shoulder joint (angle of incidence control)
- Wing twist at elbow joint
- Wing sweep at elbow joint
- Wing sweep at shoulder joint
- Spreading wing feathers (including leading edge feather control)
- Retraction and folding

Figure 2.2: An eagle uses complex wing morphing during a dive [Goldner.]

2.2.2 The History of Mimicking Avian Wing Morphing

Mimicking the wing morphing capabilities of birds with small UAVs is a relatively new area of research and has historically been challenged by weight, power, and control limitations of the electronics required to construct such vehicles. However, advances in electronics and materials have made this area of interest more accessible, and spurred study by universities.

The University of Florida flight control laboratory is home to several projects which investigate biologically-inspired flight and its application to small UAVs. This includes studying the use of variable dihedral angle, asymmetric wing sweep, and wing twist to propeller-driven aircraft [Abdulrahim 04].

Aircraft that flap for propulsion (ornithopters) are also increasing in popularity. Hobby ornithopters are commercially available, and are often sold as kits. These aircraft typically are flown using a standard RC transmitter, with flapping being used purely for propulsion (tail surfaces typically provide all directional control.) A unique ornithopter (based off of hobby aircraft) was built by a team at MIT with the goal being to eventually use the aircraft for perching experimentation. An onboard microcontroller was installed for control trials, and the aircraft has shown autonomous steady-level flight [Tedrake 09].

2.2.3 The Small Electronics Revolution and Wing Morphing UAVs

The electronics used by the hobby aircraft community are often used in the construction of small UAVs. This community tends to be continuously seeking smaller, lighter, and more powerful electronics for their model airplanes, and a market has developed to support their demand. As a result, researchers now have access to a growing supply of electronics well-suited to small UAVs, including programmable transmitters, tiny receivers, lightweight battery packs, and powerful micro-servos. The development of such compact resources is critical to building a UAV with advanced wing morphing actuation without exceeding weight limitations.

Microcontrollers (typically used by the robotics community) are becoming common-place tools in universities around the world. The growing demand for microcontrollers has driven the development of smaller, cheaper, and more powerful devices developed for robotics, but also well-suited to small UAVs. As a result, there is a growing online community of small UAV enthusiasts [DIY Drones] who use these microcontrollers in their aircraft for both research and fun. This wave of electronics advancement and the growing community knowledge base will support the development of advanced UAVs, including those utilizing wing morphing.

2.3   A Hypothesis for the Avian Landing Technique

Birds are one of the few wild animals that most people see on a regular basis: many species have adapted to city life, and there are few places on earth where birds are not present. Despite their almost continuous presence, we do not yet fully understand how they fly. To gain insight in their landing technique, videos of birds were watched to note trends in their wing positioning. This lead to a hypothesis for the avian landing technique, and the formation of a tiered research approach to learn how to apply these methods to small UAVs.

2.3.1 Video Analysis

Several videos of similarly-scaled birds landing were found, and watched in slow motion to note trends in their wing positioning. Eagles, owls, seagulls, and large parrots were the species observed. Some environmental factors were noted which were expected to affect how the animals behaved: wind direction, wind strength, and proximity to the ground were noted. Some behavior changes associated with these were noted.

If the wind was not strong, the birds would flap moments before touching down. It is postulated that at this point, the birds are flapping to create lift as 'reverse thrust' to prevent an otherwise uncomfortable collision into their perch. In cases where the wind was strong, the birds did not always flap prior to touching down. It is presumed that in this case, the wind strength was sufficient to allow the birds to 'kite', using their wings to produce lift due to the pressure caused by the wind hitting the underside of the wing.

The birds preferred landing into the wind, just as airplane pilots do. Landing into the wind reduces workload associated with maintained directional control, and reduces landing speed. This preference may be overridden in cases where such a landing approach is inconvenient, such as when crows approach to land on a wire: the birds will usually angle themselves perpendicular to the wire, regardless of the wind direction.

If the birds were landing on the ground, it was postulated that they could experience ground effect (the tendency for a wing to create less drag when flying within a wing span of the ground). Behavior changes associated with this effect were not noted, but it is recommended that any future researchers into this area of study remain aware that ground effect could be playing a role in the birds' behavior, even if it has not yet been identified.

Wing, body, and tail position were noted during the landing approach. Specifically, the following factors were observed:

- Wing dihedral angle
- Wing sweep angle
- Body angle relative to flight path

- Feathers spread (Wing and Tail)

- Wing flapping

Figure 2.3 shows a screenshot from a video of an eagle landing on a nest. The body position is noted (blue line) along with the flight path (red line.) Relative wind was also observed (white arrow.)

Figure 2.3. A screenshot from a video of an eagle landing [Getty Images.]

2.3.2   The Landing Approach

After closely watching the videos, a hypothesis for the avian landing process was formed. This is summarized as a sequence of wing morphing with body and tail positioning also noted.

- Bird approaches perch from gliding flight

  o   Forward velocity slowly decreases due to drag

- Bird sweeps wings forward slowly

  o   Causes a pitch up. Bird pitches up enough to increase body angle relative to flight path without gaining altitude.

  o   Body angle relative to flight path becomes large, and drag increases.

  o   Increased drag results in rapid decrease in forward velocity and concurrent change in relative wind.

- Bird airspeed decreases, approaches stalled condition

- Bird flaps as 'reverse thrust'

  o   Amount used varies according to wing loading/inertia and wind conditions

  o   Simultaneous source of lift

- Wing sweep is used for pitch control

- o Required to maintain desired body angle. Body angle and subsequent drag used to adjust flight path angle.

- ▪ Overall positive dihedral angle maintained

- o Inherent stability, prevents striking wings on objects near perch

- ▪ Wing twisting observed

- o Assumed aids in roll control

2.3.3   Tiered Research Approach

The biologically-inspired perching problem is inherently complex, relying on a variety of wing-morphing techniques. The effect of each individual wing-morphing method is not yet fully understood, and would aid in understanding the effects of combining these methods. Table 2.1 shows a summary of the perceived levels of historical experience, control difficulty, and construction difficulties associated with particular sub-problems of the perching problem. Construction difficulty is based upon the weight challenges associated with increased number of actuators, and control difficulty is associated with the number of parameters to control. Prop-hanging is included for comparison purposes.

Table 2.1: The relative difficulties of various aspects of the biologically-inspired perching problem.

	Historical Experience	Theoretical Control	Construction difficulty
Prop Hanging	Good	low (RC gyro can stabilize)	simple
Wing Sweep Only	Some	medium	medium
Wing Twist Only	Some	medium	medium
Wing Sweep and Wing Twist	low	hard	hard
Flapping Only (Ornithopter)	Good	low	low (available as kit)
Ornithopter with wing sweep	Very low	hard	Very hard
Ornithopter with wing twist	Very low	hard	very hard
Ornithopter with wing sweep and wing twist	Very low	very hard	very hard

A fully actuated ornithopter (using wing twist and wing sweep variation) would provide the closest approximation to a bird, and be a valuable research tool for attempting the avian perching problem. However, as implied by Table 2.1, the low levels of understanding for the sub-problems leading up to this problem indicate that it would be beneficial to use a tiered research approach: study wing morphing in more isolated circumstances before attempting the fully actuated case. The lessons learned from simpler aircraft with limited wing morphing could then be applied towards the design of an aircraft with complex wing morphing capabilities. As mentioned in the avian landing hypothesis, wing sweep variation is postulated as a pitch control method. It was also observed in several phases of the landing approach (see Figure 2.4), and could therefore be a key control method used by birds. This sub-problem of the avian perching problem was thus selected for immediate study.

Figure 2.4: A falcon displaying forward wing sweep before landing [Goldner.]

Chapter 3

Aircraft Design

3.1   Scale Selection

Before proceeding to computer modeling or experimentation, and appropriate model for study needed to be designed. An aircraft model which incorporated some biological inspiration was desired, yet the aircraft should retain conventional features for those aspects that were not critical to the study of wing sweep for pitch control. Furthermore, the aircraft model needed to be reasonable to construct and operate. This chapter will address the factors considered when designing the aircraft, and the processes used to tune the geometry.

3.1.1   Similarity to Existing Models

Similar scale models were used for general sizing of the aircraft (primarily wing area, wingspan, and weight). These models consisted of birds and hobby remote control aircraft of similar size. Hawks, owls, seagulls, and crows were some of the species used for inspiration. The average wingspan and weight for each species was obtained, and pictures of the birds in gliding flight were obtained. ImageJ [ImageJ] was then used to estimate each bird's wing area 'S' (based upon the known wingspan'b'.)The wing loading (WL) was then calculated using (3.1).With known wing area and weight (W), the aspect ratio (AR) could then be found as defined by (3.2) [Yechout 03].

$$WL = \frac{W}{S} \tag{3.1}$$

$$AR = \frac{b^2}{S} \tag{3.2}$$

The resulting values for various species were then recorded in a spreadsheet for comparison purposes. Some examples are shown in Table 3.1, along with the values for a hobby RC ornithopter called

the 'Slow Hawk 2'. These values were used to define a design space for the research model aircraft: the corresponding values for the research model would be constrained to the ranges dictated by these working models.

Table 3.1: Comparing geometry, weight, wing loading, and aspect ratio for birds and RC aircraft.

	average wingspan (in)	average weight (oz)	total wing area (in^2)	total wing area (ft^2)	wing loading (oz/ft^2)	Aspect Ratio
Barn owl	*43*	*16.2*	*263.5*	*1.826*	*8.872*	7.02
seagull	*51.1*	*20*	275.9	1.916	10.438	9.46
Slow Hawk 2	42	17	362	2.514	6.762	4.87

3.1.2 Equipment Availability

Equipment for remote controlled aircraft is not cheap, and tends to be specific to the scale and type of aircraft being built. This is particularly true for electric aircraft drive motors, servo motors, electronic speed controllers (ESC), and battery packs. If at all possible, it is preferable to reuse a working set of equipment than to invest in an entire new set of equipment. Electronics for an RC airplane was available, but the equipment on hand was meant for use on small aircraft (of about 11 oz. or less). As a result, the maximum weight of the research airplane would ideally be 11 ounces to avoid purchasing new electronics.

3.1.3 Operation Logistics and Safety

It was desirable to design an aircraft that could be flown on a small field (the size of a soccer field.) This would make finding an appropriate field for operating the aircraft easier. Safety was also a concern: large RC aircraft can cause injury to people or significant damage to property if they crash. Smaller, lighter planes are a safer option, and tend to require less powerful drive motors. Regardless, all RC aircraft must be operated with caution: future researchers are advised to refer to the advice and guidelines set forth by the Academy of Model Aeronautics (AMA) [AMA].

Large RC aircraft tend to be difficult to store, and can be easily damaged as a result of inadequate space or improper handling. This risk is more pronounced for model aircraft than other types of RC models (cars, boats, etc.) as they tend to be made from foam, balsa wood, or thin membranes susceptible to

damage. A common practice with RC aircraft is to make the wings removable, allowing the aircraft to be more easily stored. If the aircraft can fit in a protective box, risk to the aircraft is further reduced. The chance of accidental damage is higher in crowded laboratory environments, and could lead to time-consuming repairs. Therefore, an ideal design would be small, have removable wings, and fit in a box for safe storage and transportation.

3.2   Wing Design

3.2.1   General Planform

Because the focus of this project was to mimic an avian maneuver, the wing planform was selected to mimic an avian shape: straight root leading edge portion with rounded tips. Figure 3.1 shows this semi-elliptical shape in nature, as displayed by a barn owl flying overhead.

Figure 3.1: A barn owl displaying a semi-elliptical wing planform [Meyers.]

The aircraft's wing planform was tuned using a MATLAB (Matrix Laboratory) script. This script assumes that the wing area can be approximated as a rectangular leading edge portion, a triangular trailing edge portion, and a parabolic tip (see Figure 3.2.) The user inputs values defining the dimensions of these portions (wingspan and variables 'a', 'c', and 'd' as defined by Figure 3.2.) The program then calculates the resulting wing area, aspect ratio, wing loading and plots the wing planform.
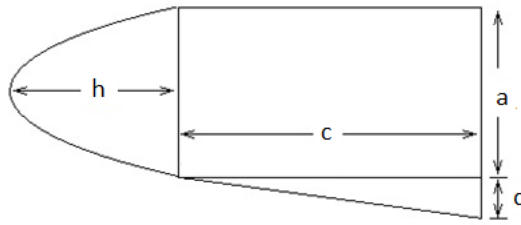
Figure 3.2: The approximation of the wing planform used in MATLAB.

The code was run with different input values until converging upon a solution which included a moderate aspect ratio and wing loading within the limits set by the similar scale models. A sample of the code output is shown in Figure 3.3 below, and the values selected using this script are summarized in Table 3.2, shown with values of some similar models for comparison.
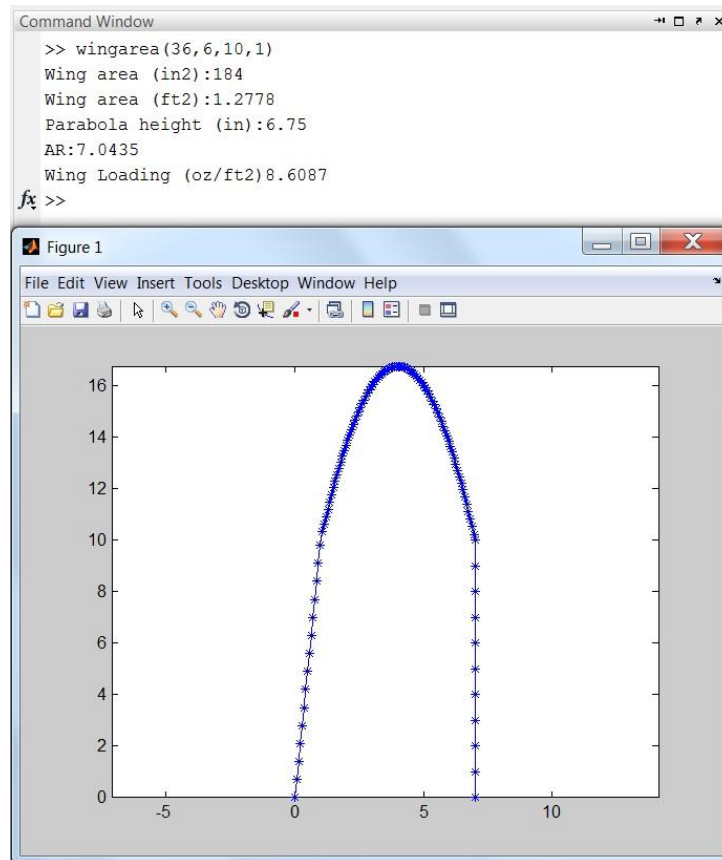
Figure 3.3: Sample output of MATLAB script to tune wing planform.

Table 3.2: Selected values for research aircraft (bottom row) and values of comparative models.

	average wingspan (in)	average weight (oz)	total wing area (in^2)	total wing area (ft^2)	wing loading (oz/ft^2)	Aspect Ratio
Barn owl	*43*	*16.2*	*263.5*	*1.826*	*8.872*	7.02
seagull	*51.1*	*20*	275.9	1.916	10.438	9.46
Slow Hawk 2	42	17	362	2.514	6.762	4.87
research model	36	11	184	1.278	8.608	7.04

After the MATLAB code had been used to select planform dimensions, the selected planform was printed out to scale. The parabolic tip was then manually tilted, and a spline curve was used to smooth the transition between the parabolic tip and the root sections. This resulted in a negligible change in area, but a smoother planform. Figure 3.4 shows the final platform.

Figure 3.4: Final wing planform after tiling parabolic tip section.

3.2.2   Airfoil Selection

A cambered airfoil similar to a bird's was desired to retain biological similarity. Birds wings consist of a thickened leading edge portion (for bone and muscle structure) and a thin trailing edge portion (feathers). Their wings are highly cambered, with exact shape varying according to species. The National Aeronautics and Space Administration (NASA) conducted some research into the shape of bird airfoils [Liu 04], including that of a barn owl: a species of comparable scale to the research aircraft. The barn owl airfoil was compared to other highly cambered airfoils used in aircraft design, and a similar airfoil (NACA5304) was selected for use.

A thickened trailing edge portion was incorporated into the aircraft airfoil, providing structural support and retaining avian similarity. In addition, the width of this thickened portion relative to the chord varies along the span, similar to a bird's wing. Figure 3.5 shows a comparison between a standard NACA5304 airfoil, a barn owl wing, and the airfoil selected for the research aircraft.
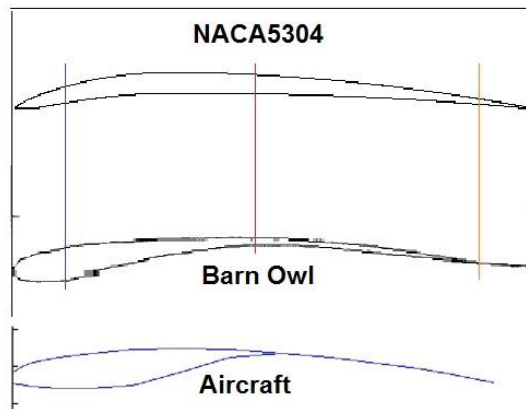
Figure 3.5: Comparison of airfoils.

To help reduce tip stall tendencies, the wing was twisted (about the leading edge) at the root by 4.5°, with this value smoothly decreasing spanwise to 0° of twist near the wing tip. This would theoretically stall the wing root prior to tip, helping to maintain aileron effectiveness when operating at high angles of attack.

3.3 Fuselage and Tail

The fuselage and tail surfaces of the aircraft were kept conventional, since the effects of wing morphing had been isolated for study. Therefore, these portions do not attempt to mimic nature, and are instead designed to be as simple, structurally sound, and lightweight as possible.

3.3.1   Structural Requirements

The fuselage needed to support the lift load transferred through the wing sweep mechanism, the thrust load from the nose-mounted propeller, and the aerodynamic loading from the tail surfaces. In addition, it needed to act as a platform for mounting the aircraft electronics. The fuselage did not need to be particularly low drag, since this aircraft was not being designed for efficient cruising flight. The simplest solution to address all of these concerns was to taper a flat a sheet of .25 thickness balsa wood to act as the main fuselage structure. This provided a solid surface to mount the wing sweep mechanism, and allowed the thrust load to run parallel to and directly through the main structure (see Figure 3.6).
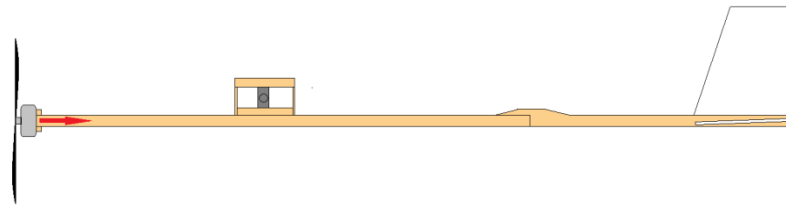
Figure 3.6: Simplified diagram fuselage with thrust directed through structure.

One of the most common forms damage associated with crashing an RC airplane is damage to the tail: this tends to occur due to tail strike on landing. To help minimize the potential damage caused by such an event, the tail boom was designed to break away at the single junction connecting the tail boom to the fuselage. In the event of a tail strike, the bond between the tail boom and the top surface of the fuselage structure would fail, resulting in the tail 'peeling off' the fuselage, hopefully without any further damage to the fuselage or tail surfaces. A breakaway on tail strike is depicted in Figure 3.7.
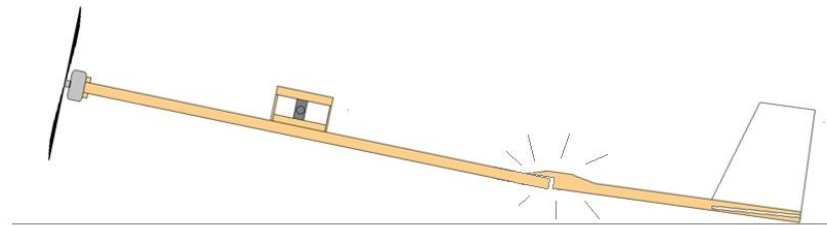
Figure 3.7: Simplified diagram of a tail strike, with breakaway joint failing.

3.3.2   Tail Surface Sizing

Tail surface geometry is similar to RC aircraft of similar size: simple rectangular planform with approximately the last third of the surface hinged. Sizing of the vertical stabilizer and rudder were simply based on other models, but the horizontal stabilizer was more tuned using Athena Vortex Lattice (AVL), a simplistic Computational Fluid Dynamics (CFD) program. This program was used for further analysis purposes, and will be discussed in more detail in chapter 4. Essentially, this program can predict how a given aircraft geometry will perform. With the basic aircraft geometry input into AVL, the elevator effectiveness could be evaluated. The horizontal stabilizer size, stabilizer angle of incidence, and elevator sizes were adjusted in AVL until the elevator was predicted to be able to trim the aircraft (cause a zero pitching moment.) The resulting angle of incidence was set at 3.5°, with the planform geometry shown in Figure 3.8.
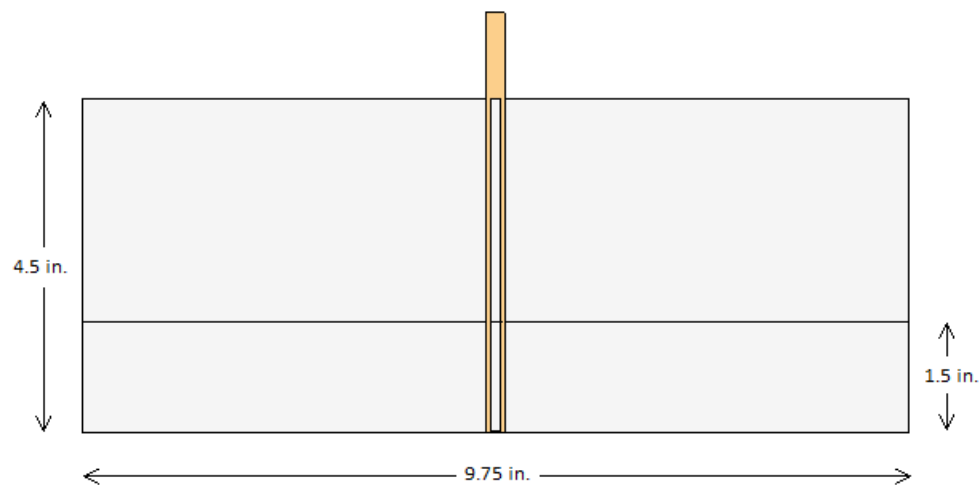
Figure 3.8: Horizontal tail geometry.

Chapter 4

Computer Model Analysis

Computer analysis of the aircraft geometry described in chapter 3 was performed to determine the effect of wing sweep on pitch response. The programs used to perform this analysis will be introduced, and the analysis process outlined. The analysis results will then be presented and discussed.

4.1 Introduction to Athena Vortex Lattice

A simplistic Computational Fluid Dynamics (CFD) program called Athena Vortex Lattice (AVL) (mentioned briefly in chapter 3) was used to predict the effect of wing sweep variation on pitch response. This program was developed at the Massachusetts Institute of Technology (MIT), and uses an extended vortex lattice model to predict lifting surface behavior of rigid aircraft [Drela]. Aircraft geometry and mass properties are dictated by specifically-formatted input files.

4.1.1 Input Requirements

Two input files are required in order to run an AVL analysis: a geometry file (indicated by a .avl file extension) and a mass file (indicated by a .mass file extension). These files must be formatted in a way that is recognizable by AVL; exact formatting guidelines are provided in the AVL documentation. The parameters defined in these files include:

- Flow velocity (Mach Number)
- Wing area
- Reference chord
- Reference wing span
- Center of mass location
- Approximate coefficient of drag
- Lifting surface geometry

- o Includes wings and tail sections

- o Defined as several sections along span

- o Includes airfoil geometry

- o Permits control surface declarations

- Body geometry

 - o Body surface approximated as a curve revolved around axis

Generally, the AVL input files are written using a text editor, and the file extension is changed as needed. For this project, a MATLAB script (to be discussed in more detail later) produced both input files.

4.1.2   Desired Output

AVL can be used for a variety of situations, from designing a new aircraft to predicting performance of an existing model. For this project, AVL was used for two primary purposes: sizing of the horizontal stabilizer (as discussed in chapter 3), and predicting the aircraft pitching moment coefficient ($C_{m,tot}$). This dimensionless parameter relates the total aircraft pitching moment to the flow conditions and aircraft geometry as described by (4.1) (where 'q' is dynamic pressure, 'S' is wing area, and 'c' is representative chord length.). A positive value ($C_{m,tot} > 0$) indicates a nose-up pitching behavior, while a negative value ($C_{m,tot} < 0$) indicates nose-down pitching behavior. A value of zero indicates a trimmed longitudinal flight condition (no pitching action.)

$$C_{m,tot} = \frac{M_A}{qSc} \qquad (4.1)$$

In addition, AVL was used to record the neutral point (NP) location of the current geometry. This value describes the center of gravity location which would result in neutral longitudinal static stability. When the center of gravity location (X_{CG}) and neutral point location (X_{NP}) are known, the static margin (SM) can be found as described in (4.2) [Yechout 03.]

$$SM = X_{NP} - X_{CG} \qquad (4.2)$$

A positive static margin indicates positive longitudinal static stability (stable configuration.) If the CG is moved at of the NP, the SM will become negative, indicating a longitudinally unstable configuration. For this analysis, the coordinate system was defined with the datum at the leading edge of the unswept wing with the positive x axis extending downwind and the positive y axis extending out the right wing (see Figure 4.1.)
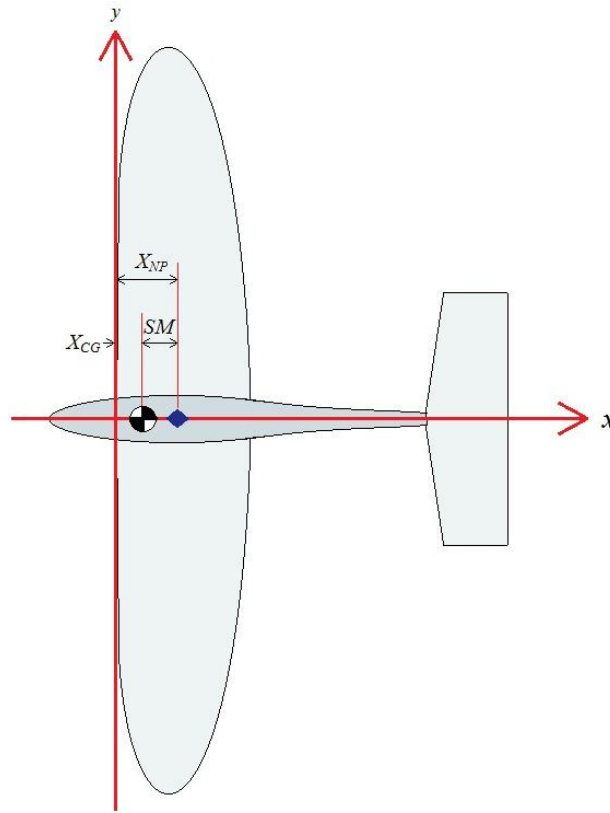
Figure 4.1: Coordinate system with CG location, NP location, and SM definition.

Sizing of the horizontal stabilizer was a small task, and did not require extensive preparation to perform: the tail parameters were manually edited using a text editor. Preparation for the pitching moment analysis was much more in depth, requiring the use of a sophisticated MATLAB code. The goal of this analysis was to produce a plot of pitching moment coefficient versus wing sweep angle, thus indicating how the aircraft would respond with different wing sweep cases.

4.2   MATLAB Code

4.2.1   Building the MATLAB Plane

As discussed earlier, AVL requires a geometry input file prior to performing an analysis. This file must contain the wing geometry data as a sequence of connected sections along the span, each with their own position and airfoil data. These sections must be defined parallel to the flow (parallel to the fuselage.) Therefore, the section geometry will change depending upon wing sweep angle: as the wing is swept forward or backwards, the section 'seen' by the flow will change. In Figure 4.2, the section 'seen' by the flow over the unswept wing is shown as the red line, and is different from the section 'seen' by the flow over the swept wing (the blue line.)
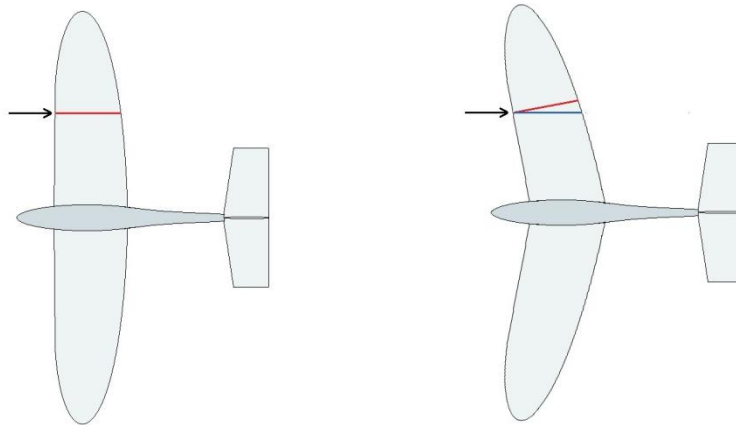
Figure 4.2: Perceived section change with wing sweep

This change in the perceived section geometry as a result of wing sweep required that the geometry of the wing written to the AVL input files change according to wing sweep angle. A MATLAB script was used to handle this task: the script accepts wing sweep angle as an input parameter, calculates the spanwise section properties corresponding to that sweep condition, and writes the corresponding geometry to the AVL input files.

4.2.2 Coordinate Transformation Matrix

Calculating the swept wing geometry required that the unswept wing geometry be hard-coded into the script. The unswept wing geometry was written into MATLAB as a matrix, with each row corresponding to a wing section. The columns then contained data about section position (relative to the origin), chord length, and angle of incidence. In addition, the airfoil shape for each section was stored as a text file. The known airfoil shape and section properties were then used to construct a mesh of points representing the surface of the unswept wing, each with their own (x, y, z) coordinate. The script then used a coordinate transformation matrix (4.3), the given desired sweep angle (w), and the known constant dihedral angle (d) to generate a new mesh of points corresponding to the swept wing surface.

$$
\begin{bmatrix} x' \\ y' \\ z' \end{bmatrix} = \begin{bmatrix} \cos(w) & -\sin(w) & 0 \\ \cos(d)\sin(w) & \cos(d)\cos(w) & sin(d) \\ -\sin(d)\sin(w) & -\sin(d)\cos(w) & \cos(d) \end{bmatrix} \begin{bmatrix} x \\ y \\ z \end{bmatrix} \tag{4.3}
$$
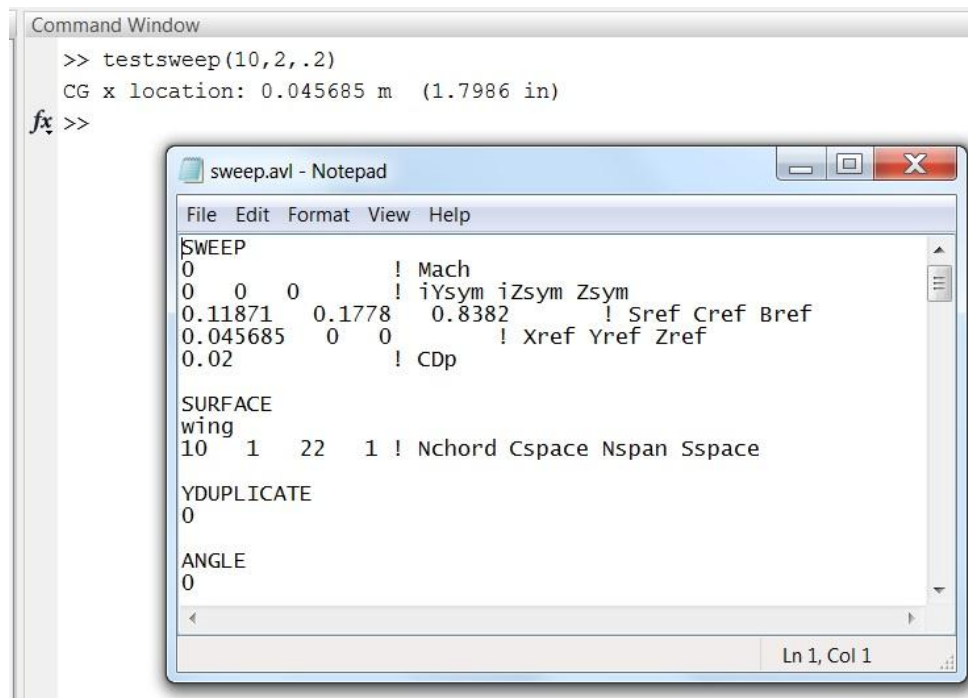
After rotating the mesh of points, new sections parallel to the flow were extracted. The MATLAB script used these new sections to define the wing geometry in the AVL input file, completing the wing geometry calculation effort.

After calculating the wing geometry, the MATLAB script calculated the center of gravity of the aircraft and wrote this into the AVL mass input file. This calculation assumed that the fuselage mass was constant, but the mass of the wings had moved. It calculated the new center of gravity location, and then represented the total aircraft mass as a point mass at the center of gravity (CG) location.

4.2.3 User Interaction and Code Output

The MATLAB script was called from the MATLAB command window, with three input parameters: wing sweep angle (in degrees), camber value, goal spacing. The camber value was held constant for all test cases, and was used primarily for debugging purposes (changing between the avian airfoil and a simpler airfoil). The goal spacing parameter is a parameter specifying the desired spacing between wing sections, and was held constant for all test cases.

Once the code is run, it will output the calculated CG position (as referenced from the origin, defined as the location of the leading edge of the wing in the unswept configuration.) This output is primarily to verify that the code has run: the same CG location is written to the text files. Although the script has not displayed much information in the command window, it has written two text files: sweep.avl and sweep.mass. Sample command window output and a portion of the resulting sweep.avl file is shown in Figure 4.3 below.

Figure 4.3: Command window output from MATLAB, and a portion of the resulting sweep.avl file.

4.3   Using AVL

This section will provide a brief overview of how AVL was used for this project; it is not intended to be a comprehensive guide for using AVL. For further details on AVL, please refer to the AVL documentation. Sample files are also available online, along with AVL itself.

4.3.1   Setup in AVL

Prior to running an analysis, the input files must be generated using the 'testsweep' MATLAB script. The script must be called prior to opening AVL, and the files generated by MATLAB must be in the same directory as the AVL.exe application.

Once the input files have been generated, AVL is executed and it displays a text prompt. The following commands are used to load the geometry and mass files:

        AVL   c>   load sweep.avl

        AVL   c>   mass sweep.mass

        AVL   c>   mset 0

The command "mset 0" is used to indicate that the same mass file should be used for all run cases (only applies for cases using the same geometry file.)

After loading the geometry and mass files, the geometry is checked using AVL's geometry plot option. This visual representation of the aircraft is useful to verify that the MATLAB code correctly generated the swept wing geometry. This function is accessed using the following command prompts:

        AVL   c>   oper

        .OPER (case1/1)   c>   G

        Geometry plot command: CA

        Geometry plot command: k

The 'G' command will enter the geometry menu, and display the current aircraft configuration (see Figure 4.4 for example.) 'CA' command will display chord lines, and the 'k' command will activate the keystroke mode. In this mode, the model can be moved using the 'l', 'r', 'u', and 'd' keys to examine the geometry.
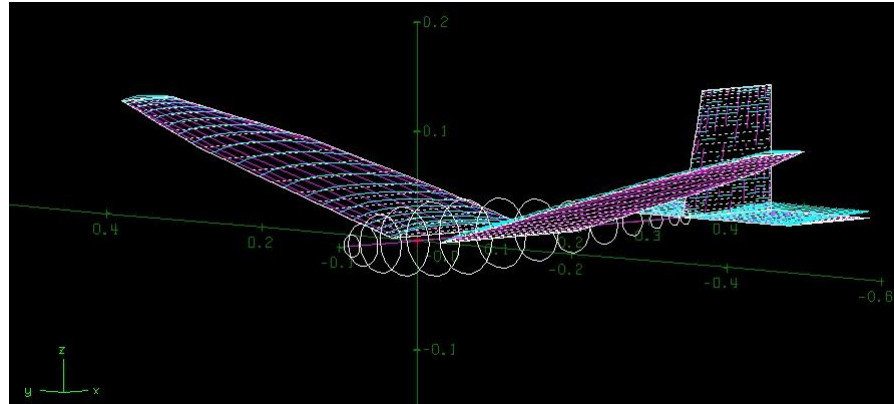
Figure 4.4: Visual representation of aircraft using the AVL geometry plot function.

Prior to beginning an analysis, the aircraft velocity is specified. This is accessed from the OPER menu, through the 'C1' submenu:

.**OPER (case1/1)**   **c>**   C1

Enter parameter, value (or # - + N)   **c>**   v   2.68

The C1 menu prompts for a value to be specified. Entering 'v 2.68' constrains the velocity to 2.68 length units/time units (m/s for this project.)

After setting the velocity, the angle of attack (AOA, usually represented by α) is specified from the OPER menu. The below command tells AVL to adjust AOA to keep AOA constant at 0 degrees:

.**OPER (case1/1)**   **c>**   A   A   0

Prior to running any analysis, the elevator was used to trim the aircraft to zero pitching moment. AVL was used to find the requisite amount of deflection to achieve this goal for the unswept wing case, and then this deflection amount was held constant for all other cases. This would be similar to the procedure used by a pilot flying an RC model: trim the aircraft first using elevator, then begin experimentation. During experimentation, the elevator should not be adjusted as this would corrupt pitch response data. Trimming the aircraft in AVL is performed from the OPER menu:

.**OPER (case1/1)**   **c>**   D1   PM   0

.**OPER (case1/1)**   **c>**   x

The first command indicates that the elevator (d1) will be constrained to produce a neutral pitching moment (pm). The 'x' command tells AVL to execute the run case. AVL then displays a list of values corresponding to the predicted aircraft response, including the elevator deflection. The output is shown in Figure 4.5, with the predicted elevator deflection value displayed at the bottom (indicating approximately -6 degrees of deflection, trailing edge up, is required to trim.)

```
.OPER (case 1/1)   c>  x
 Building normalwash AIC matrix...
 Factoring normalwash AIC matrix...
 Building source+doublet strength AIC matrix...
 Building source+doublet velocity AIC matrix...
 Building bound-vortex velocity matrix...

iter d(alpha)  d(beta)   d(pb/2U)   d(qc/2U)   d(rb/2U)   elevator
  1  0.585E-07  0.000E+00  0.000E+00  0.000E+00  0.000E+00 -0.596E+01
  2 -0.586E-07  0.000E+00  0.000E+00  0.000E+00  0.000E+00  0.196E-02
  3  0.688E-10  0.000E+00  0.000E+00  0.000E+00  0.000E+00 -0.875E-06
-------------------------------------------------------------------
Vortex Lattice Output -- Total Forces

Configuration: SWEEP
    # Surfaces =   7
    # Strips   = 132
    # Vortices =1320

 Sref = 0.11871      Cref = 0.17780      Bref = 0.83820
 Xref = 0.48491E-01  Yref =  0.0000      Zref =  0.0000

Standard axis orientation,  X fwd, Z down

Run case:  -unnamed-

 Alpha =    0.00000     pb/2U =    0.00000     p'b/2U =   0.00000
 Beta  =    0.00000     qc/2U =    0.00000
 Mach  =     0.000      rb/2U =    0.00000     r'b/2U =   0.00000

 CXtot =   -0.06969     Cltot =    0.00000     Cl'tot =   0.00000
 CYtot =    0.00000     Cmtot =    0.00000
 CZtot =   -0.55705     Cntot =    0.00000     Cn'tot =   0.00000

 CLtot =    0.55705
 CDtot =    0.06969
 CDvis =    0.02000     CDind =    0.04969
 CLff  =    0.54854     CDff  =    0.05061    | Trefftz
 CYff  =    0.00000         e =     0.3198    | Plane

  elevator        =  -5.96158
```

Figure 4.5: AVL output from an elevator trimming case.

After a run case has been executed, the predicted neutral point value can be accessed from the OPER menu:

.**OPER (case1/1)** **c>** st

This command will display a list of stability-axis derivatives, with the predicted neutral point value displayed at the bottom.

4.3.2 Running the Pitching Moment Analysis

A procedure was used to perform a pitching moment analysis, requiring both MATLAB and AVL. This procedure uses the AVL and MATLAB commands discussed in the previous sections, and applies them for wing sweep cases ranging from -10° (backward sweep) to 16° (forward sweep) . Sample visual representations from these sweep cases are shown in Figure 4.6.

1) Run the MATLAB script for the desired wing sweep angle

2) Open AVL and load the new sweep.avl and mass.avl files

3) Setup the run case

    a. Check geometry plot, velocity, and AOA

    b. Verify correct elevator deflection

4) Execute the run case

5) Record the total pitching moment coefficient

6) Record the neutral point

7) Repeat process for new wing sweep angle
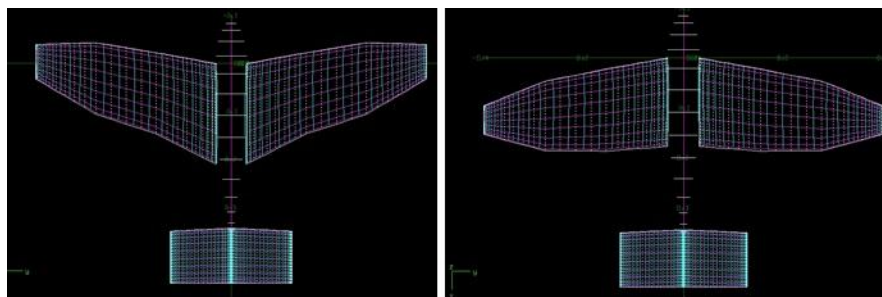
Figure 4.6: AVL graphical representation of wing sweep cases.

The pitching moment and neutral point values obtained during the pitching moment analysis were recorded in an excel spreadsheet, along with the corresponding wing sweep angles. This allowed the data to be easily plotted, aiding in identification of trends.

4.4 AVL Results

4.4.1 Pitching Moment Analysis

The total pitching moment coefficient values obtained from the AVL pitching moment analysis were plotted versus wing sweep as seen in Graph 4.1. Pitching moment values increased as the wings were swept forward (positive wing sweep angles) and decreased as the wings were moved backward (negative wing sweep angles). A linear trend line was computed which closely approximated the series (an R^2 value of .9875).

Graph 4.1: Total pitching moment coefficient versus wing sweep as predicted by AVL.
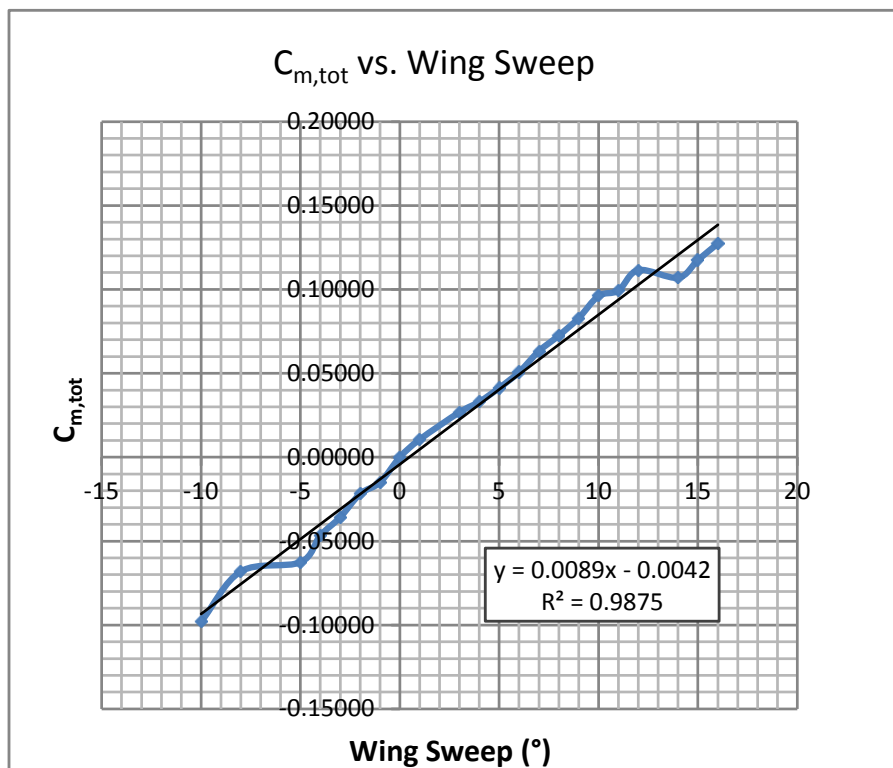
A positive pitching moment corresponds to nose-up pitching tendency, while a negative pitching moment corresponds to nose-down pitching behavior (see Figure 4.7). Therefore, this analysis predicts that forward wing sweep will induce a nose-up pitching behavior, while backward wing sweep will induce a nose-down pitching behavior. This supports the hypothesis that wing sweep can be used for pitch control, and justifies the construction of an experimental prototype for further investigation.

$$C_{m,tot} < 0 \qquad C_{m,tot} > 0$$
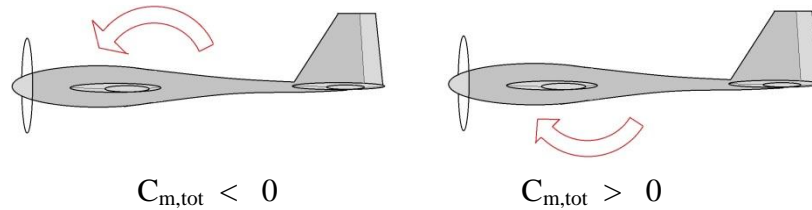
Figure 4.7: Pitching moment coefficient sign convention

4.4.2 Static Margin Analysis

The static margin values obtained from the pitching moment analysis were plotted versus wing sweep angle, along with the center of gravity location (see Graph 4.2.)

Graph 4.2: Static margin and center of gravity versus wing sweep angle.
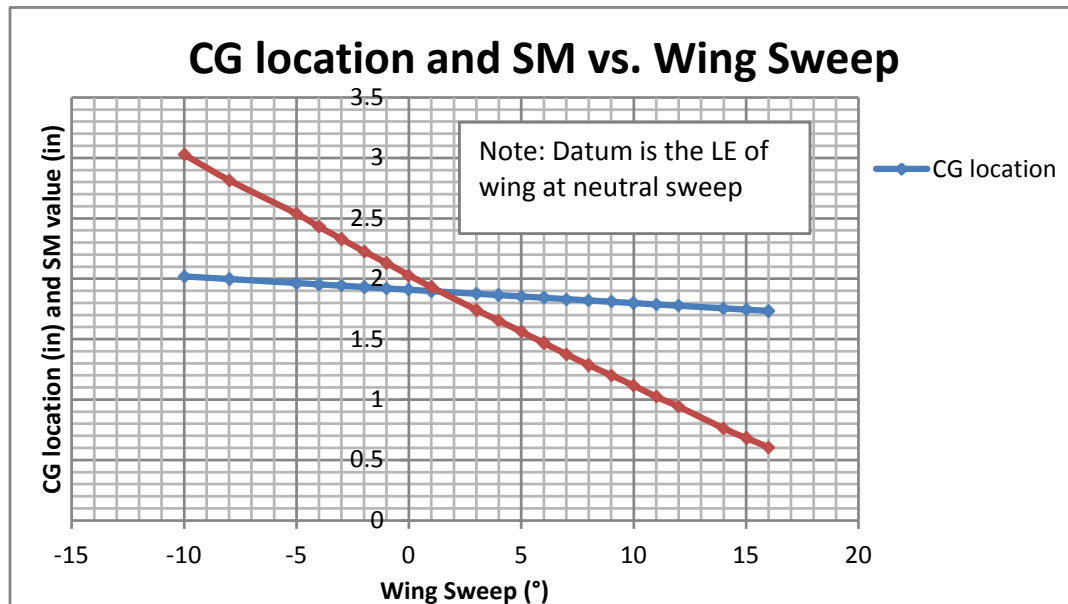
As the wings were swept forward, a decrease in static margin is predicted. As the wings swept backward, an increase in static margin is observed. The static margin values remained positive, predicting that longitudinal static stability would be maintained [Yechout 03]. Center of gravity followed a similar trend: as the wings swept forward, the CG location moved forward (resulting in a decrease in CG value). As the wings swept backward, the CG location moved backward (resulting in an increase in CG value).

Chapter 5

Experimental Prototype

Computer modeling indicated that wing sweep causes a change in pitching moment coefficient; supporting the hypothesis that wing sweep can be used for pitch control. To further investigate this hypothesis, an experimental prototype was constructed. This chapter will outline the construction process (including composite construction techniques), and describe the hardware used on the aircraft.

Note to future researchers: use extreme caution when working with bladed hand tools, shop equipment, and composites. If you are not familiar with a tool, seek guidance before proceeding. Always use sharp blades: they require less force to use, reducing the risk of a blade slipping while cutting. When working with composites, avoid skin contact and breathing in fumes. Sanding and cutting should be done in a well-ventilated area or under a fume hood to avoid breathing in fine particles. Wear a mask when working with fiberglass microbeads (a fine glass dust used to thicken epoxy) to reduce risk of inhalation. This chapter is not intended to be a comprehensive guide to working with hand tools, shop equipment, or composites. Please be careful.

5.1   Fuselage Construction

The fuselage and tail surfaces are conventional in design (see Figure 5.1) and were built using materials common to RC aircraft: balsa wood, bass wood, and cell foam (white foam sheet used for tail surfaces.) The fuselage main structure was built from a sheet of .25 in. thick balsa, with a tail boom cut from .25 in. balsa. Cuts were made either by hand with an exacto knife or using a band saw.
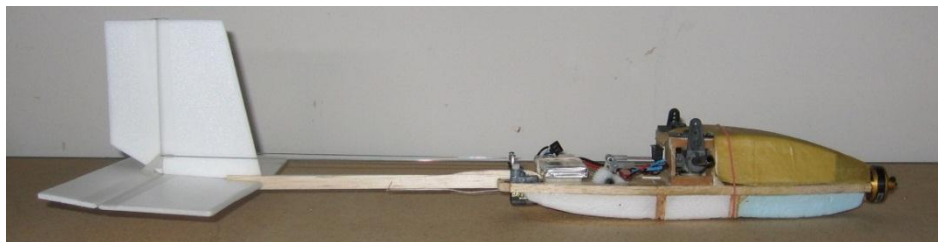
Figure 5.1: Complete aircraft fuselage.

The fuselage varies from standard RC aircraft fuselages in that it includes a complex shoulder joint assembly for the wing sweep mechanism (see Figure 5.2). The supporting joint structure was constructed from basswood (denser and stronger than balsa), and attached to the main fuselage balsa plank using a mixture of epoxy and microbeads. In addition, a layer of lightweight fiberglass was applied to the structure's attachment points to aid in load transfer to the fuselage.
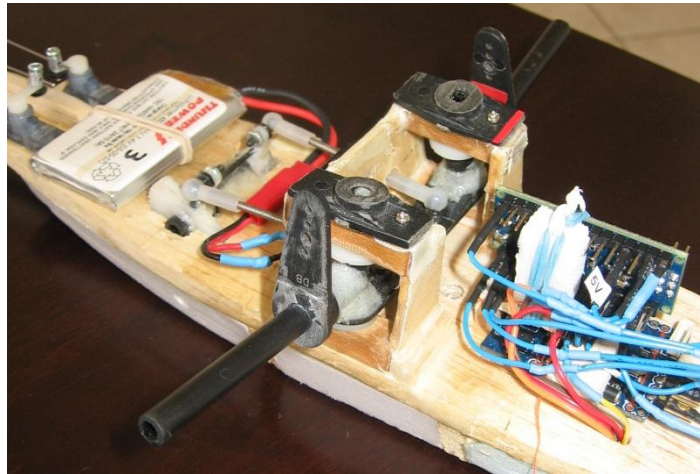
Figure 5.2: Close-up of aircraft shoulder joint assembly.

The fuselage was not designed for aerodynamic efficiency, and is not a streamlined design. The extra complexity of constructing a streamlined fuselage was not considered necessary, since the aircraft was not required to be aerodynamically efficient to perform its job as a research platform (in comparison to aircraft that require endurance or gliding performance.) However, it was considered important to design a canopy to direct the propwash away from the electronics in the nose. To save weight, a Kevlar canopy was constructed. This was made by hand using a simple wet layup process. First, a foam mold was carved to the desired canopy shape. The mold was carefully covered with a cheap and simple release film solution: packaging tape (see Figure 5.3). Waxed paper was used to protect the clamps and table from the epoxy.

Figure 5.3: Foam mold prepared for wet layup process.

A single layer of Kevlar was wetted with epoxy and draped over the mold, and pins were used to hold the material to the mold shape (see Figure 5.4.) The part was left to cure for 24 hours.

Figure 5.4: Kevlar pinned to foam mold.

After cure was complete, the pins were removed and the Kevlar was released from the mold. Excess material was trimmed by hand using scissors and exacto knives. Thin foam was applied to the inside of the side walls to add additional rigidity, helping the structure to fit snugly on the fuselage. The resulting structure was flexible and rugged, which would help it to survive any abuse received during flight testing. Total weight was .1 ounces. (See Figure 5.5).

Figure 5.5: Completed canopy.

5.2 Wing Construction

The biomimetic wings were complex to construct, and did not follow standard RC aircraft construction practices. The wings included several demanding features: curvature in two directions (resulting from camber and wing twist), thin membrane structure, and the requirement to be supported only at a single point (the shoulder attachment point.) In addition, it was desired to make the wings removable to protect them during storage and transportation. Composite materials were used to meet these demands, along with a modified version of a thin membrane design approach developed at the University of Florida [Abdulrahim 04].

The wings would be composed of two parts: a thin upper surface, and a thickened foam portion underneath. The thin upper surface was built using a wet layup process on custom-built molds. The thicker foam portion was cut from foam sheet by hand, using templates printed from MATLAB. The upper surfaces and foam portions were then glued together with epoxy. Details regarding the construction processes for both the thin upper surface and the thicker foam portions will be addressed in the following sections.

5.2.1 Mold Construction

The thin upper surfaces required the construction of custom molds which held the shape of the wing. Because the wings required curvature in two directions, a hotwire approach would not be sufficient. Furthermore, a milling machine was not available for this purpose. The last feasible, low-budget option was to construct the molds by hand from a sheet of 1 inch thick blue insulation foam (available at hardware

stores). This dense foam cuts readily with a bandsaw, and can be easily sanded. Fiberglass will adhere to the surface, making it a suitable material for the mold.

A MATLAB script was used to calculate and plot the airfoil shape at one inch increments along the wingspan (see Figure 5.6). The resulting airfoil shapes were printed to scale, and carefully labeled and cut out into templates for use in the mold construction process.

Chord 5: 3.5 deg rotation
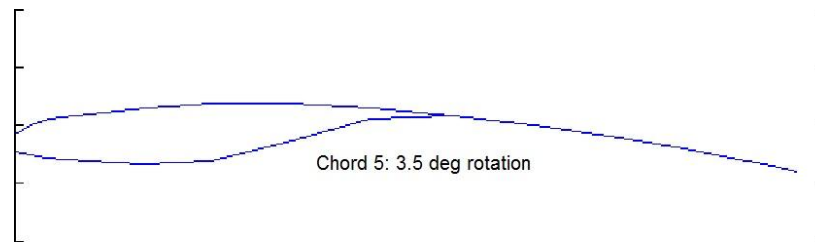
Figure 5.6: An airfoil template generated by MATLAB.

Each template was traced onto the blue foam, leaving a flat bottom surface but retaining the airfoil shape for the top surface. The sections were then cut out with a bandsaw to within a blade's width accuracy. As each section was cut, it was stacked next to its neighboring sections (see Figure 5.7).
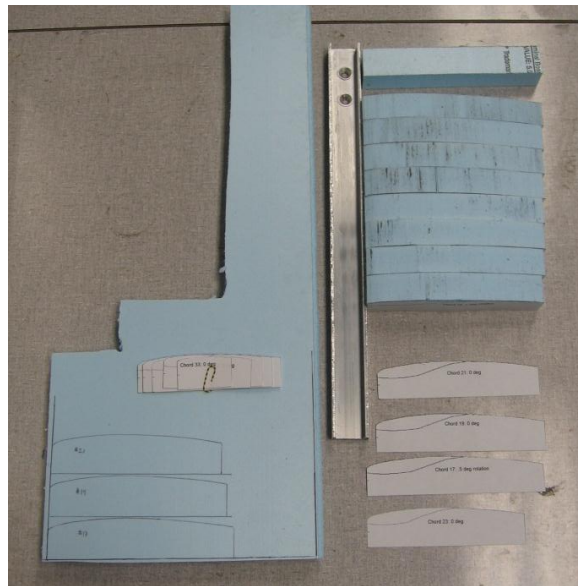
Figure 5.7: Mold templates being traced, cut out, and stacked together.

The wing planforms for both wings were printed out to scale, and each was glued to a piece of wood to provide a solid base for the molds. As each foam section was cut out, it was compared to the corresponding section for the other wing. If a discrepancy was noticed, the offending section was discarded and a new piece cut. After passing this test, each piece was placed on top of the planform printouts (see Figure 5.8).
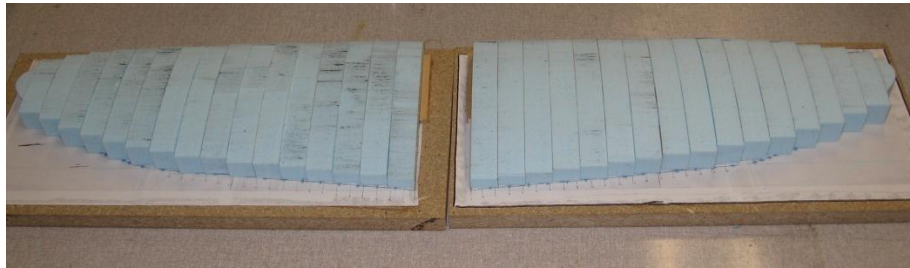
Figure 5.8: Foam sections stacked together

Once all pieces had been cut from the foam sheet, the leading and trailing edges were cut to match the planform shape. After this, the foam pieces were permanently glued to the wooden bases (on top of the planform papers.) The top surface was then sanded to smooth the transitions between foam sections, being careful not to over-sand (see Figure 5.9.)
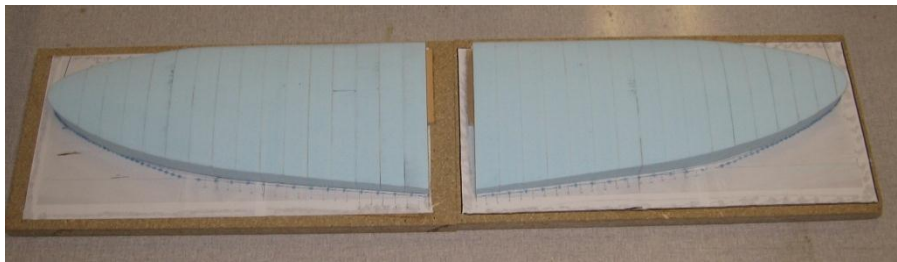
Figure 5.9: Foam sections glued to bases and sanded smooth.

Once the foam sections were glued and sanded, they were holding the shape of the wing top surfaces. However, they were not rigid enough to withstand the pressure that would be exerted on them during a vacuum bagging process. In order to prevent the foam from deforming during vacuum bagging, two layers of lightweight (2 ounce), fine weave bi-directional fiberglass were applied using a wet layup process. After the fiberglass had cured, it was sanded to a smooth finish to remove any bumps. Guidelines

were then drawn to aid in the wing wet layup process: these marks indicated where the carbon strips and fiberglass layers should be placed (see Figure 5.10.)

Figure 5.10: Completed molds with fiberglass applied and guidelines drawn.

5.2.2   Wet Layup

Once the molds were complete, the top surfaces of the wings could be constructed using a standard wet layup process. Each wing was constructed separately: this was primarily to avoid making mistakes which could result from rushing to complete both wings before the epoxy began curing. Additionally, it minimized the amount of lab space needed for the procedure.

The mold was placed on a large, clean metal plate which would provide a smooth surface for sealing the vacuum bag. Release film was then taped on top of the mold to prevent the composite part from adhering to the mold (see Figure 5.11).
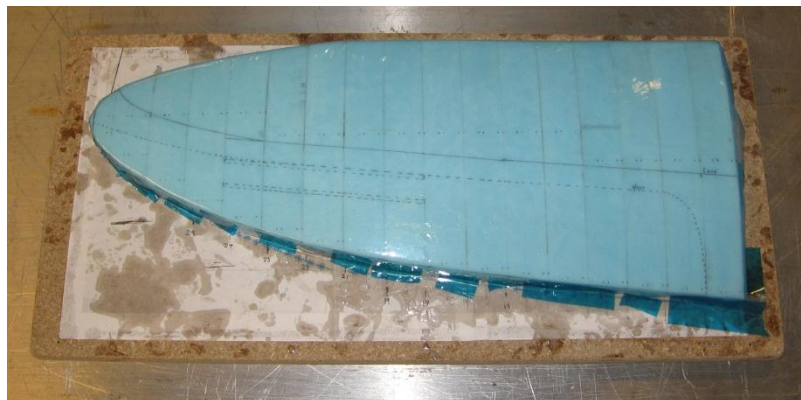
Figure 5.11: Release film stretched over mold.

The carbon strips, fiberglass sheets, and rip-stop nylon were all cut to shape and laid out on the table prior to mixing the epoxy. This would reduce workload during the open time (the time in which the epoxy can be spread [West Systems]). To aid in spacing these strips, 3/8 inch wide tape strips were applied to the mold between the regions where the carbon strips would lay. These were also intended to prevent excess epoxy from spreading onto the areas where bare rip-stop nylon would lie (see Figure 5.12).

Figure 5.12: Materials cut and prepared for wet layup.

The epoxy system used was West Systems 105 resin with 206 slow-cure hardener. This is an industrial-strength epoxy which is readily available at boating stores, and can be mixed by weight or by volume. The 206 hardener was selected because it permits a long pot life (approximately 25 minutes of working time), valuable time when delicately placing carbon strips. The resulting epoxy cures to a solid state in 10 to 15 hours [West Systems]. The epoxy was mixed in a resin to hardener ratio of 5 to 1 by weight. The epoxy was then spread onto the carbon and fiberglass on a plastic sheet to the side of the mold: this prevented spreading excess epoxy on the mold.

The carbon strips were wetted on the plastic sheet, then carefully placed into position between the tape strips on the mold. After all the chord-wise strips had been placed, the tape was carefully removed and

discarded. The spanwise aileron strips were then placed, being careful not to move the chord-wise strips. (See Figure 5.13.)
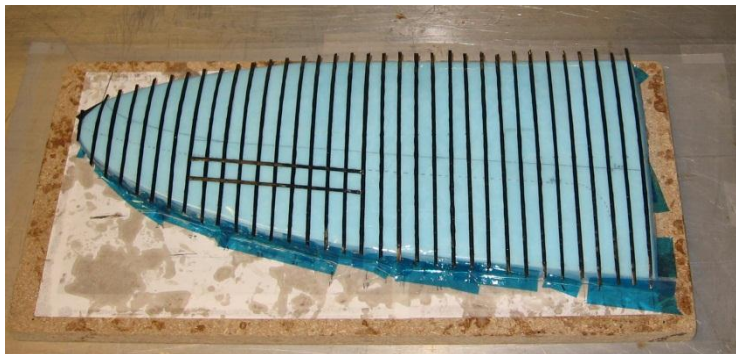
Figure 5.13: Carbon strips applied to mold.

Two layers of lightweight (2 ounce) fine-weave bidirectional fiberglass were applied next. These added stiffness to the most highly-cambered portions of the wing, and also provided structural support in the spanwise direction. Furthermore, the fiberglass sheets would provide an appropriate surface for gluing the bottom foam structure. To aid in torsional stiffness, each sheet was cut to 45 degrees, such that the leading edge of the wing was 45 degrees from the weave direction. The glass was wetted on the plastic sheeting next to the mold (see Figure 5.14), then carefully transferred to mold using the mold guidelines for alignment (see Figure 5.15).

Figure 5.14: Fiberglass sheet being wetted on plastic.

Figure 5.15: Fiberglass applied to mold (wetted glass is clear).

A layer or rip-stop nylon was applied on top of the fiberglass layers (see Figure 5.16). This durable material is used in the construction of paragliders, and will resist tearing. For this aircraft, it allows some flexibility between the carbon strips of the wings, mimicking the flexibility of bird feathers. In addition, the bright red cloth increases visibility, an important consideration for a small aircraft being flown under manual control.

Figure 5.16: Rip-stop nylon applied on top of carbon strips and fiberglass layers.

After the rip-stop nylon was in place, the vacuum bagging process began. First, a sheet of peel ply was draped over the part (see Figure 5.17). This cloth acts as a release film, preventing the vacuum bag

materials from sticking to the part. In addition, its porosity permits excess resin to be pulled through the cloth, and soaked into the next layer of cloth (the breather cloth).

Figure 5.17: Peel ply draped over the part.

Once the peel ply was in place, a generous piece of breather cloth was draped over the entire mold (see Figure 5.18). This cloth would soak up excess resin, and provide a path for air to escape while pulling the vacuum. In addition, it would help to ensure a uniform pressure distribution across the part during the curing process. Extra breather cloth was folded and placed next to the part edge: this was to allow adequate airflow to the vacuum port, which would be placed directly on the cloth.

Figure 5.18: Breather cloth draped over the mold.

Sealant tape was carefully applied to the metal plate, making sure to include some vertical tape protrusions near the corners of the mold. These protrusions would help the vacuum bag plastic to accommodate the three-dimensional mold. Once the sealant tape was in place, the inner portion of the

vacuum port was placed next to the mold and the vacuum bag plastic was carefully tacked into place. A small hole was cut in the vacuum bag, and the outer portion of the vacuum port was installed over this hole. The vacuum was then applied, and pressure changes observed on a vacuum gauge. Any significant pressure changes indicated the presence of leaks, which were hunted down and sealed. Once all leaks had been addressed, the part was left to cure (see Figure 5.19).

Figure 5.19: Part curing in a vacuum bag.

After the cure was complete, the vacuum was released and the vacuum bag removed (see Figure 5.20). The breather cloth and peel ply were removed (see Figure 5.21), revealing the cured wing top surface (see Figure 5.22). The wing surface was lifted off the mold successfully, with the mold release film still stuck to the under surface of the wing (see Figure 5.23).

Figure 5.20: Vacuum bag removed, before removing breather cloth and peel ply.

Figure 5.21: Removing breather cloth and peel ply.

Figure 5.22: Part after vacuum bagging cloth removed.

Figure 5.23: Underside of part, before removing release film.

The release film easily peeled off the underside of the wing, revealing a smooth surface (see Figure 5.24.) The finished part held the desired shape of the wing top surface, but had some excess material on the edges where it had overlapped the mold. This excess material was later trimmed by hand.

Figure 5.24: Part after removing release film.

After successfully building the left wing, the process was repeated to construct the right wing using the other mold (see Figure 5.25). The molds were not damaged in the process, and successfully held the wing shape during the vacuum bagging process.
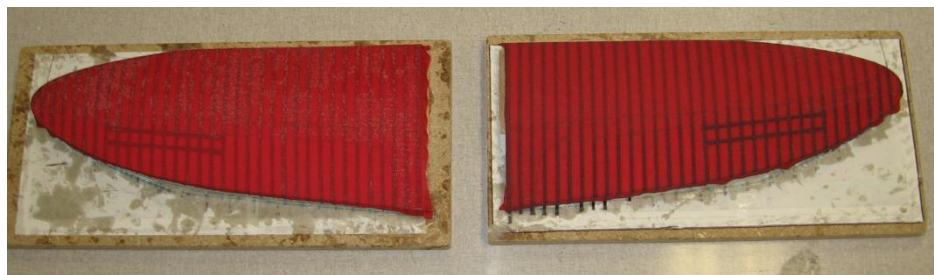
Figure 5.25: Completed wing top surfaces sitting on their molds.

5.2.3   Bottom Foam Structure

After completing the top wing surfaces, the bottom wing foam structures were built. These were constructed using a process very similar to the mold construction process: MATLAB templates were traced onto 1 inch thick foam, and the sections were cut by hand using a band saw. The resulting foam sections were stacked together, and the edges between neighboring sections sanded smooth (see Figure 5.26). A hole was drilled in the innermost sections, which would later be used to mount a carbon rod for attachment to the fuselage. In addition, the innermost foam section was extended to provide some additional support, and prevent the trailing edge from flexing excessively due to the lift load.

Figure 5.26: Building the bottom foam structure.

After all the foam sections had been cut and glued together, the foam structure was ready to be glued to the wing upper surface. However, the upper surface of the wing was smooth as a result of the release film, and was not an ideal surface for adhering epoxy. To address this issue, the area which would contact the foam structure was sanded to provide some surface roughness. Afterwards, the foam structure was glued to the wing upper surface using epoxy. A layer of lightweight fiberglass was then applied over the foam structure to protect it from minor impact.

5.2.4   Attachment Points

The wings were designed to be removable, and also to be hinged at one shoulder joint. To meet both requirements, a single carbon tube was inserted and glued into the foam structure of the wings at the approximate quarter chord position. This tube acted as the main spar, and also as the main attachment mechanism: it would slide onto a concentric carbon rod fixed to the fuselage shoulder joint. Modified heavy duty servo horns were glued (using a mixture of epoxy and microbeads) to both the fuselage and wing sides: when the wing tube slid onto the fuselage carbon rod, the servo horns lined up when the wing was at the correct angle of incidence. Screwing the servo horns together would then ensure correct alignment, as well as secure the wings to the fuselage (see Figure 5.27).
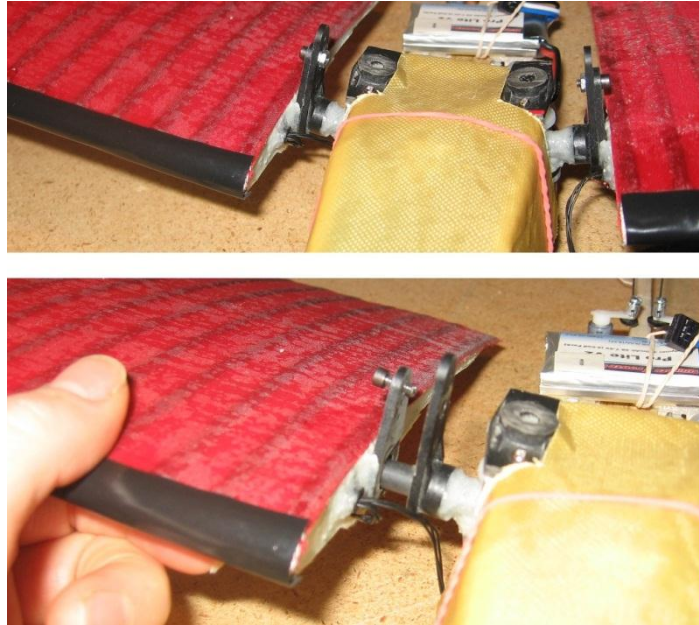
Figure 5.27: Securing the wing to the fuselage.

5.2.5   Ailerons

The ailerons were conventional, and cut from the carbon strips applied during the wet layup process. A sharp blade was used to cut through the carbon strips along their midline for the aileron edges. The carbon strip which bounded the top portion of the aileron was not completely cut through, but cut just enough to act as a hinge. A piece of medical tape was then applied across the top surface, reinforcing the hinge. (Medical tape is commonly used as the sole hinge for small RC aircraft control surfaces.) The resulting structure was thin, fit snugly with the rest of the wing, and retained the desired camber. Micro servos imbedded into the foam structures of each wing actuated the ailerons (see Figure 5.28). The final weight of each wing was 1.75 ounces, including the servo weight.

Figure 5.28: Completed wings with ailerons and attachment points.

5.3   Wing Sweep Transmission

Wing sweep was controlled by a single servo on the fuselage, with wings being swept simultaneously and symmetrically. The transmission required was custom made and built by hand, using a variety of off the shelf RC aircraft components and carbon tubing.

Each wing had a known mass of 1.75 ounces, with the center of gravity approximately inches from the wing root. Each wing was spaced .75 inches from the fuselage side to allow clearance while sweeping. To approximate the torque exerted from the wings, some calculations were performed with the assumption that the weight of the wings was causing a moment about the center of rotation (see Figure 5.29). This would be akin to the aircraft in a vertical climb (not an expected behavior), and would place a high degree of stress on the servo. Heavy duty servo horns would be used to provide moment arms, and their known lengths are included in calculations.
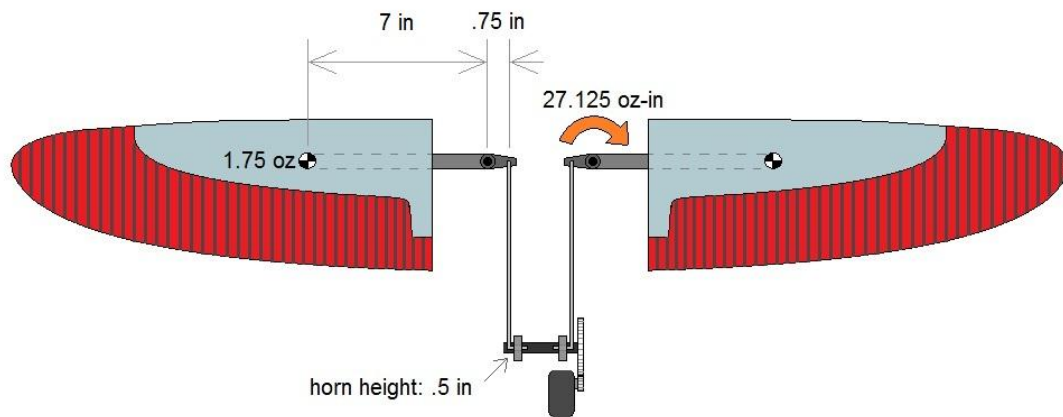
Figure 5.29: Simplified torque analysis diagram.

As shown in Figure 5.29, the torque exerted by each wing mass is calculated as the wing weight multiplied by the moment arm. This value is multiplied by two to represent the torque applied by both wings, as in (5.1).

$$(7.75 \text{ in})(1.75\text{oz})(2) \ = \ 27.125 \text{ oz} - \text{in} \tag{5.1}$$

This is the torque which the servo transmission must apply in the opposite direction in order to maintain static equilibrium. A HiTec HS5085 Metal Gear servo was selected for the job: this servo is capable of producing 59.7 oz-in of torque at a rate of .13 sec/60° [Hitec.] This satisfies the requirement to hold the weight of the wings in a vertical climb, and the extra available torque would safely overpower the effects of drag. It was desired to use the full servo travel range (90°) to produce the full wing sweep range (~40°). This requirement dictated the selection of the gear ratio between the servo and wing sweep transmission. Because the servo horns used for moment arms on the wing shoulder joints and wing sweep transmission were identical in length, the travel range of the transmission gear would be identical to the travel range of the wings. Therefore, the wing travel range would be determined by the gear ratio between the servo gear and the transmission gear. This ratio is represented by (5.2), with the variables 'R' and 'r' as described in Figure 5.30.

$$\frac{R}{r} = \frac{90°}{\theta} \tag{5.2}$$
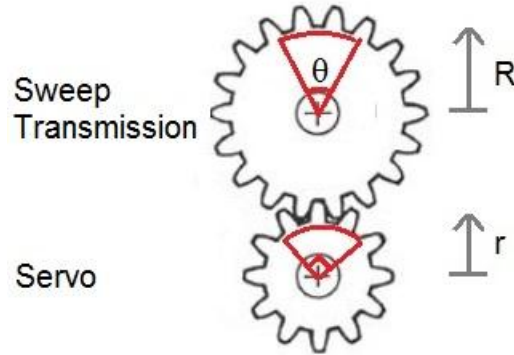
Figure 5.30: Gear ratio schematic.

Table 5.1 shows a range of values for θ, and the corresponding gear ratios. Gear ratios of 2 or 2.25 would permit the servo to actuate the wings across the full 40° of travel.

Table 5.1: Sweep gear travel range and corresponding gear ratios.

θ (°)	R/r
45	2
40	2.25
35	2.57
30	3

A gear ratio of 2 was selected as the final design: this ratio was commercially available with a spline matching the servo motor, and fulfilled the sweep range requirements. The extra range of travel could be limited using the adjustable travel volume (ATV) feature of the radio transmitter, preventing any potential interference problems.

The shoulder portion of the wing sweep mechanism (see Figure 5.31) was constructed using concentric carbon fiber tubing, heavy duty servo horns and nylon washers. The joint was built at a fixed 15° dihedral angle to improve roll stability. A 'T' shaped carbon tubing structure was created, with the small portion rotating about a fixed carbon rod and the longer portion supporting the wing (see Figure 5.32).

Creating this structure required cutting the carbon tubing with a sharp hand saw: this is recommended over band saws because it is less likely to accidentally split the tubing during cutting. The sections which would be joined with epoxy were carefully sanded (see Figure 5.33) to add surface roughness. This improved the bond between the epoxy and the carbon tubing, strengthening the joint. An epoxy and microbead mixture was then used to join the carbon tubing at a 90° angle.
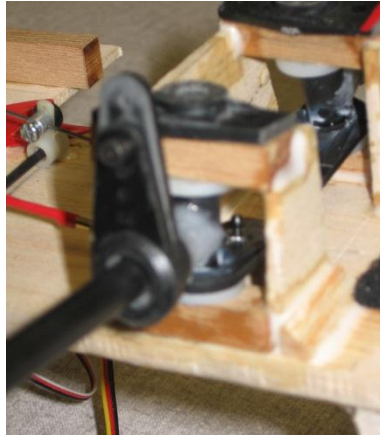
Figure 5.31: Assembled shoulder structure

Figure 5.32: Carbon shoulder joint components
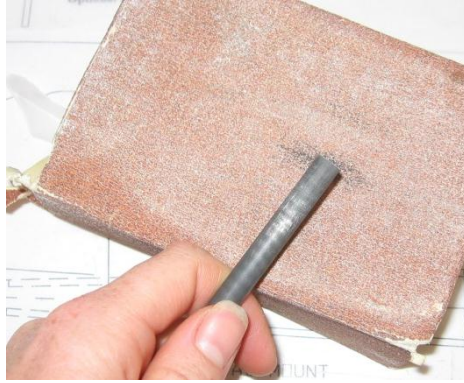
Figure 5.33: Sanding carbon tubing to improve epoxy bonding.

Nylon washers were used to space the carbon tubing off of the wooded shoulder support structure: these allowed free rotation without permitting vertical translation of the T-shaped carbon structure. Heavy-duty servo horns were glued to the wing support rod, acting as wing alignment tools and attachment points (shown in Figure 5.32 above). Another servo horn on this same structure acted as a moment arm for the wing sweep transmission. In addition, the carbon rod acting as the shoulder axis was glued to a heavy servo horn, and the servo horn could be screwed into the wooden shoulder structure. This feature permitted the shoulder joint to be disassembled without breaking any epoxy bonds, facilitating construction and repair (see Figure 5.34).
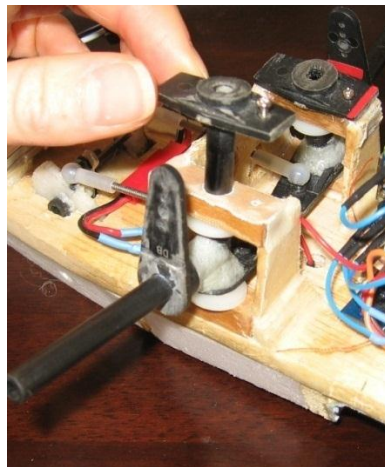
Figure 5.34: Removable shoulder joint axis permits easy construction and repair.

The transmission for the wing sweep mechanism required two servo horns (acting as moment arms) to simultaneously rotate about a fixed axis, driven by a single gear. This assembly was built using concentric carbon tubing and nylon servo horns (see Figure 5.35). Small diameter carbon rods were used to pin the servo horns to the rotating carbon rod (shown in Figure 5.35). This ensured that the servo arms remained fixed during gluing, and provided additional surfaces for the glue bond to adhere. The transmission gear pinned in a similar fashion. All components were then glued with epoxy.
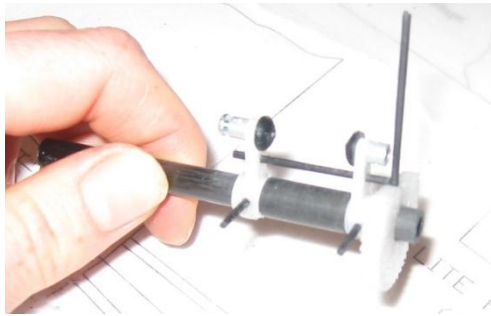
Figure 5.35: Transmission axis pinned for gluing (note that ball joints have not yet been installed.)

The rods connecting the wing moment arms to the transmission axis moment arms needed to permit some rotation, and it was desired that their length be adjustable to permit fine-tuning the wing sweep. Threaded rods with ball joints on both ends were selected for this purpose, and are shown in Figure 5.36. The entire structure was glued to the fuselage with epoxy, and small piece of lightweight fiberglass was laid over the connection to help transfer the load to the fuselage.
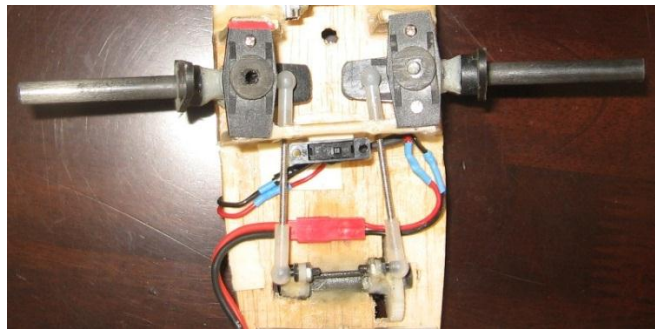
Figure 5.36: Installed transmission with threaded rod connection to wings.

The wing sweep servo was installed underneath main fuselage structure, and connected to the transmission gear through a hole in the fuselage (see Figure 5.37).
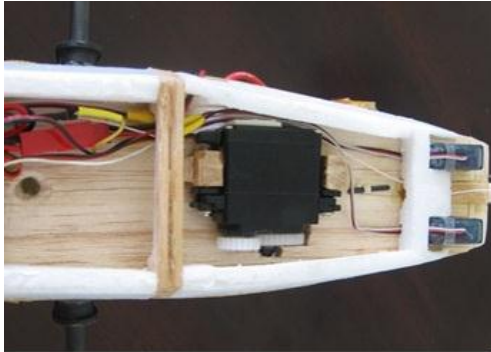
Figure 5.37: Wing sweep servo installed on bottom of main fuselage structure.

5.4   Flight Control Surfaces

Primary flight control surfaces were aileron, rudder, and elevator (not including the experimental wing sweep control.) These standard flight control surfaces were included to allow full control of the aircraft during flight testing, permitting the pilot to fly the aircraft as a normal RC airplane until wing sweep actuation.

Construction of the ailerons did not follow standard RC construction techniques, as described in section 5.2.5. However, the rudder and elevator (see Figure 5.38) were constructed following standard construction techniques, and made from common materials (flat closed-cell foam and balsa wood.) The tail surfaces were cut using a sharp exacto knife, and glued to the balsa tail boom with fast-setting cyanoacrylate (CA) glue. Medical tape was used to hinge the flight control surfaces, and two blue arrow micro servos installed on the aft fuselage controlled the rudder and elevator.
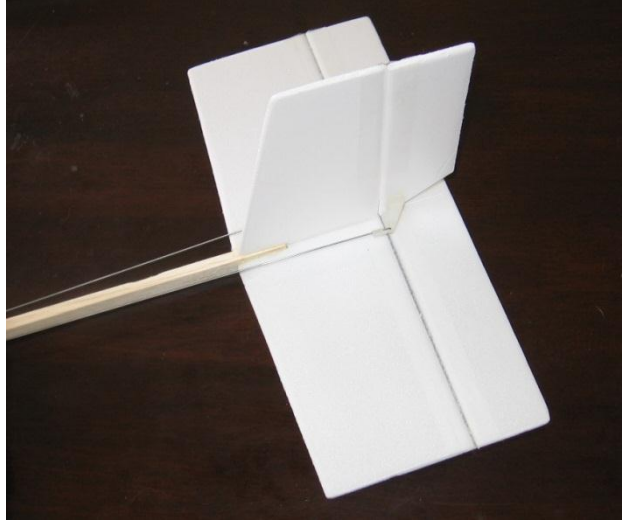
Figure 5.38: Flat foam tail surfaces.

5.5   Electronics

The electronics onboard the aircraft can be divided into two categories: standard RC electronics, and customized microcontroller components.

5.5.1   Standard RC Electronics

The aircraft was flown as a standard RC aircraft, and relied upon off the shelf RC components. A Futaba 8UAPS 8 channel transmitter was used for controlling the aircraft. The RC components onboard the aircraft used are summarized in Table 5.2, along with their function.

Table 5.2: RC components onboard aircraft

Quantity	Component	Function
1	AXI 2204/54 Goldline Brushless Motor	Propulsion
1	Castle Creations Phoenix 10 Electronic Speed Controller (ESC)	Motor speed controller
3	Thunder Power Pro Lite V2 7.4 V 480 mAh Lithium Polymer battery	Powers all electronics (interchangeable, only one onboard aircraft at a time)
1	Castle Creations Berg 7P	7 channel radio receiver
1	HiTec HS5085 MG servo	wing sweep servo
4	Blue Arrow 4.3 gram micro servo	servos for ailerons, rudder, and elevator

The receiver and ESC were installed in the nose of the aircraft, underneath the main fuselage structure (see Figure 5.39). The motor was installed on the nose on the aircraft, in a standard puller configuration.

Figure 5.39: RC electronics in nose of aircraft

5.5.2   Microcontroller Hardware

The onboard microcontroller system was used for data acquisition and closed-loop testing of the sweep control system. The individual components were purchased from online retailers, but the system required custom wiring, soldering, and programming in order to function. The components are listed in Table 5.3, along with their function.

Table 5.3: Onboard microcontroller system components.

Quantity	Component	Function
1	Arduino Nano V3.0 Microcontroller	Data Acquisition and PID Controller
1	ArduIMU V2 Flat Inertial Measurement Unit (IMU)	Acquire pitch angle, transmit to microcontroller
1	Adafruit microSD shield	Allow data storage to microSD card
1	2 GB micro SD card	onboard data storage device

The microcontroller system was mounted in the nose of the aircraft, underneath the Kevlar canopy. The IMU was installed flat against the fuselage structure: this was required to allow it to accurately record the aircraft pitch angle. The microcontroller sat above the IMU, and the SD card shied was mounted directly behind the motor (see Figure 5.40).
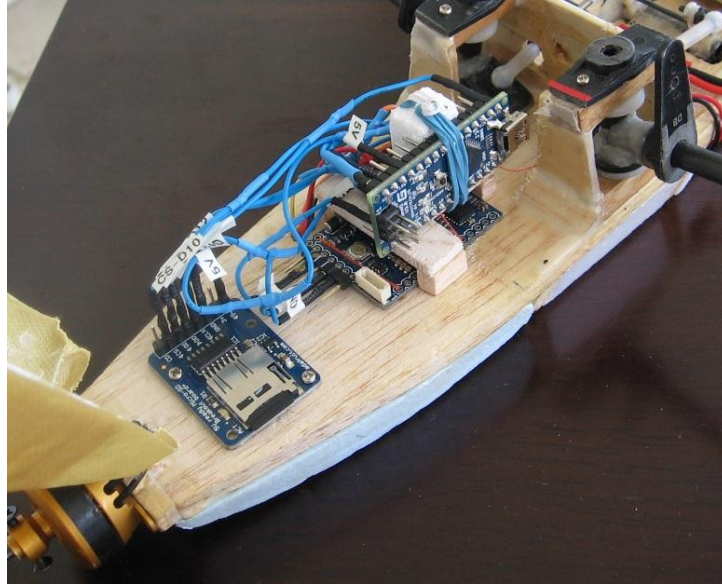
Figure 5.40: Microcontroller system components in nose of aircraft.

Chapter 6

Arduino Control System

The onboard microcontroller system had two primary purposes: record flight data, and attempt closed-loop pitch control using wing sweep. To satisfy these requirements, the code for the microcontroller allowed selection between two modes: manual flight control mode, and proportional integral derivative (PID) controller mode. The desired mode was selected in the microcontroller code before flight. This chapter will describe both modes in detail.

6.1   Manual Flight Control Mode

Before experimenting with PID control, the aircraft response to wing sweep was observed using manual control of the wing sweep angle. The pilot could command wing sweep angle from the transmitter, and the microcontroller system could be turned on and off from the transmitter. In this mode, the microcontroller system acted as a flight data recorder to record wing sweep angle and pitch angle.

6.1.1   Servo Signal Theory

The arduino monitored the signals being output from the radio receiver, and recorded these signals. Each channel of the receiver output a different signal, each intended to command a servo motor. Servo motors are usually controlled using a Pulse Width Modulation (PWM) signal which is output from the RC receiver. This signal can be represented as a square wave repeating at a known frequency, with the width of the square wave varying (see Figure 6.1). The width of this wave (measured as the time interval between amplitude rise and fall) is translated by the servo as the commanded position. A short pulse indicates one extreme servo position, while a long pulse indicates the other extreme servo position.
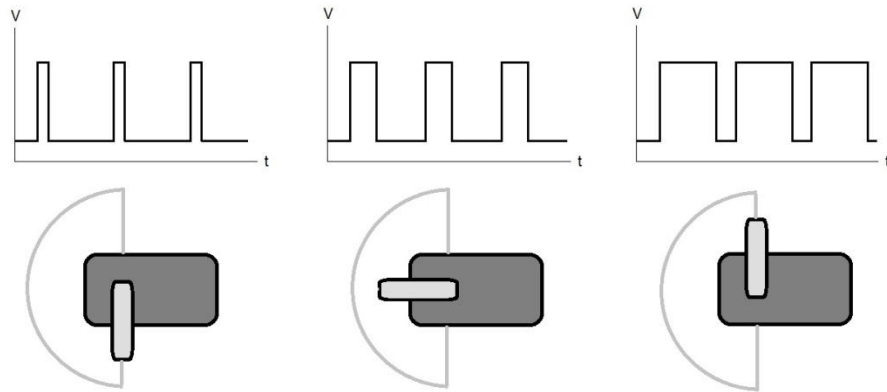
Figure 6.1: PWM servo signal and corresponding arm position.

An oscilloscope was used to observe the PWM signals being output from the RC receiver, and to measure the pulse widths corresponding to extreme servo positions (see Figure 6.2). This information was hard coded into the arduino's code, giving it reference points for calculating servo positions. When the pilot commanded the wing sweep servo from the transmitter, the RC receiver would output this command to the wing sweep servo as a PWM signal. The arduino would store the PWM value, and the wing sweep angle was then calculated using the known extreme values for the wing sweep servo PWM signals. Using the same procedure, the arduino also monitored the elevator servo position. In addition, the pilot would use a switch on the transmitter (usually used to raise and lower landing gear) to command the arduino to begin data recording. The arduino monitored the RC receiver channel corresponding to this switch, and would begin recording when sensing a jump in the pulse width on that channel.
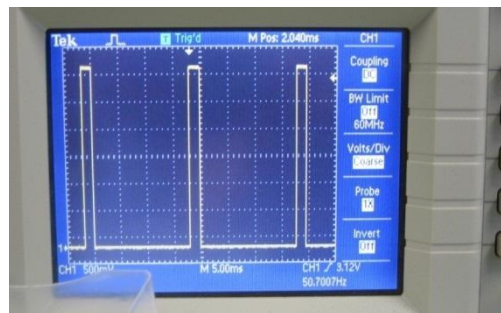
Figure 6.2: PWM signal being output from RC receiver.

6.1.2   Manual Mode Hardware Connections

In manual flight control mode, the arduino microcontroller system was wired as shown in Figure 6.3. The signal from the receiver's switch channel (usually used as an on/off signal to control landing gear position) was fed directly to the arduino. The power and ground connections from this channel were used to power the arduino. The power for the microSD shield and IMU was supplied from the arduino (with all components operating at 5 V). The signals from the receiver to the elevator and sweep servos were split, with one wire going to the servo as usual and one wire fed to the arduino. Power to the servos came directly from the receiver.
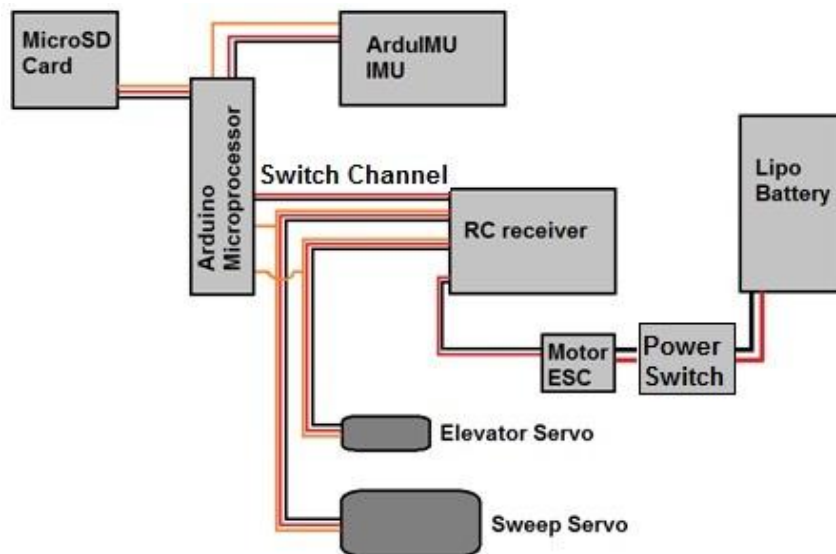
Figure 6.3: Hardware connection diagram for manual sweep control mode.

6.1.3   Manual Mode User Interaction

Operating the arduino system in manual mode was performed using a switch on the RC transmitter (see Figure 6.4). This switch is usually used for operating landing gear, but was used to signal the arduino to begin or stop recording data. Wing sweep position was selected by a knob on the transmitter.

Figure 6.4: The RC transmitter set up for manual sweep control.

Data output from the manual control mode was in the form of a text file with four data sets for each test performed:

- One value representing test start time (described as milliseconds passed from aircraft power on)

- A column of PWM values for the wing sweep servo

- A column of PWM values for the elevator servo

- A column for values corresponding to the pitch angle reading from the IMU

6.2   PID Controller Mode

After the arduino had been used for manual sweep control, it was used to attempt close-loop pitch stabilization using wing sweep as the input. This required that the PID mode be enabled in the arduino code prior to flight, and the connections to the wing sweep servo adjusted to allow the arduino to command the device. This mode was intended as an initial investigation into the concept of closed-loop pitch control using wing sweep, and thus a simple PID controller was sufficient for this purpose.

6.2.1 PID Control Theory

PID controllers are combinations of proportional (P), integral (I), and derivative (D) controllers. These controllers use feedback control to attempt to drive the current state to the desired state [DiStefano 95]. As described is [DiStefano 95], the output u_{PID} of a PID controller with input e(t) is of the form given in (6.1).

$$u_{PID} = K_P e + K_D \frac{de}{dt} + K_I \int e(t)dt \qquad (6.1)$$

The values K_P, K_D, and K_I are the proportional, derivative, and integral gains respectively. These values are used to tune the system, and adjust performance metric such as rise time, settling, time, steady state error, and overshoot (as shown in Figure 6.5). In Figure 6.5, the blue line represents a response with overshoot and settling; while the red line represents a response with undershoot. The value at m represents the desired state, the value of (m-n) represents the steady state error for the red line, point a is the rise time for the blue line, and point b is the settling time for the blue line [Denewiler 11]. An ideal system would immediately jump to point 'm', without any delay, overshoot, or undershoot. This is an unrealistic response; generally a response similar to the red line or blue line is observed. Therefore, the objective of controller tuning is approximate the ideal response as closely as possible, by minimizing rise time, settling time, and overshoot/undershoot. Various methods are available to tune PID controllers, including a simple trial and error approach: the gains K_P, K_I and K_D are adjusted until a desired system response is observed [Dorf 05.]
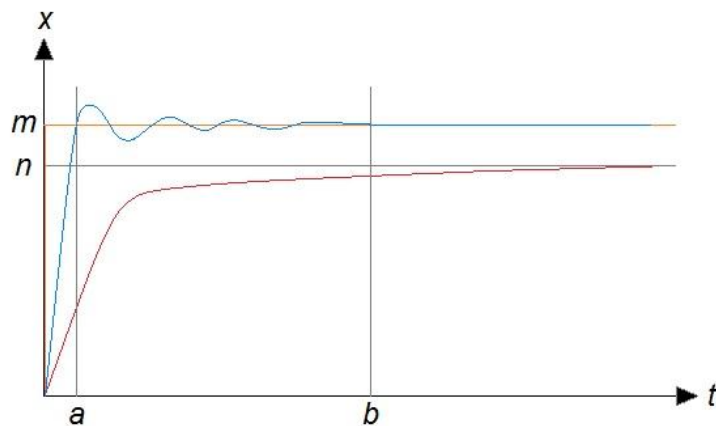
Figure 6.5: Representation of PID responses with overshoot and undershoot.

6.2.2   PID Controller Design

The PID controller used for the aircraft was designed using system identification. This is a data-driven process used to build a mathematical representation of a system which is not easily modeled by other methods. Data is acquired experimentally, and then used to represent the system dynamics. The manual sweep control flight tests were used to gather data for this purpose (flight testing and resulting data will be discussed in further detail in Chapter 7). Once the data was obtained, it was fed into the MATLAB system identification toolbox to generate an approximate model of the aircraft dynamics. The gains K_P, K_I, and K_D were then tuned experimentally until an acceptable response was predicted (see Graph 6.1).

Graph 6.1: MATLAB output of predicted system response.
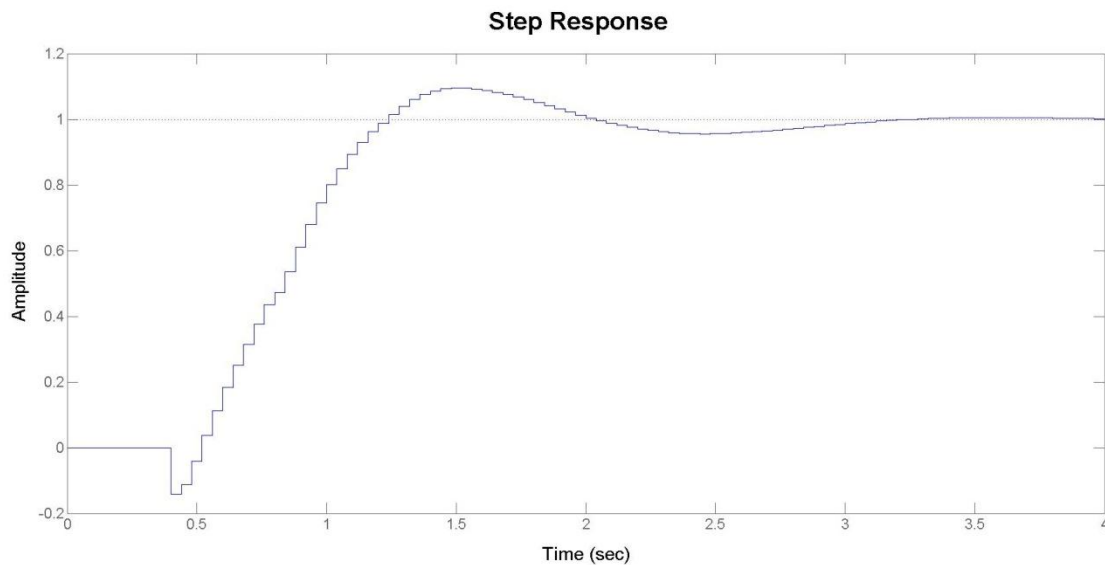
This predicted a rise time of approximately .75 seconds, and a settling time of about 3 seconds. The gains used for this controller are summarized in Table 6.1.

Table 6.1: PID Control Gains.

Gain	Value
K_P	0.243142
K_I	0.23745
K_D	0.00011154

These were the values used for the initial PID control flight test. Further tuning of the system was planned, pending the acquisition of more flight test data. The first set of data used for system identification was a short data set, and thus was expected to provide a limited model of the system. However, this still provided a starting point to build off of. The acquisition of more representative data sets could then be used to improve system modeling and minimize settling time, overshoot, and rise time. Acquiring such a data set would require modifying flight test procedures: this will be discussed in more detail in Chapter 8.

6.2.3   PID Mode Hardware Connections

The connections for the PID control mode are almost identical to the connections for the manual control mode, with one exception: the sweep servo signal wire is directly connected to the arduino, and is no longer connected to the RC receiver (see Figure 6.6). Power for the sweep servo is still pulled directly from the RC receiver.
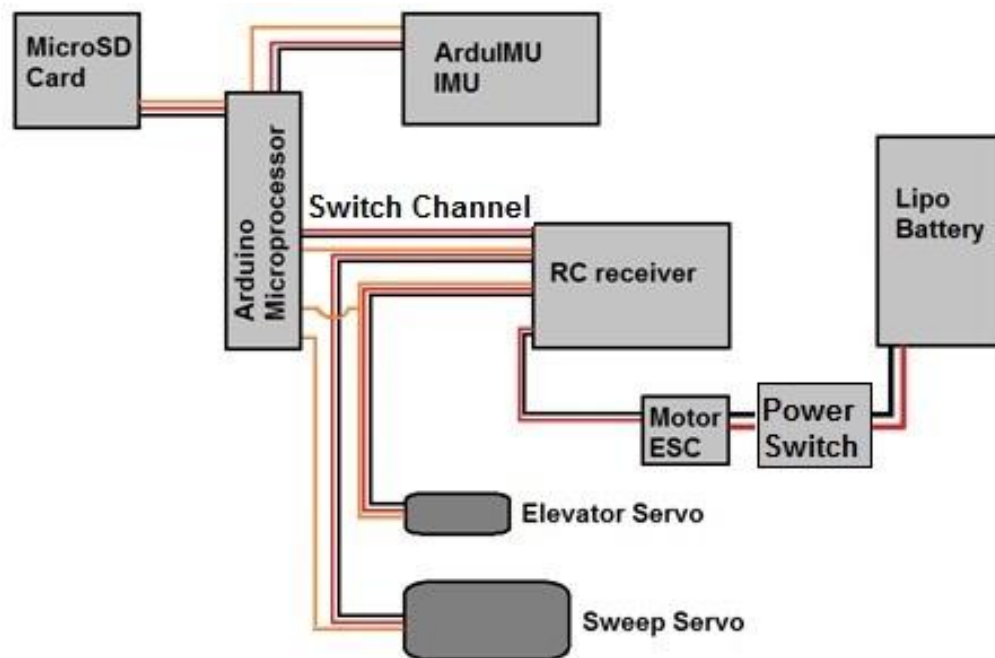
Figure 6.6: Relevant hardware connections for arduino system in PID control mode.

6.2.4   PID Mode User Interaction

Prior to flight, the PID mode had to be enabled in the arduino code, and the wing sweep servo connected directly to the arduino. The switch on the transmitter previously used to enable arduino data recording was used to active PID control, and the knob previously used for manually selecting wing sweep angle was now used to select desired pitch angle (see Figure 6.7).
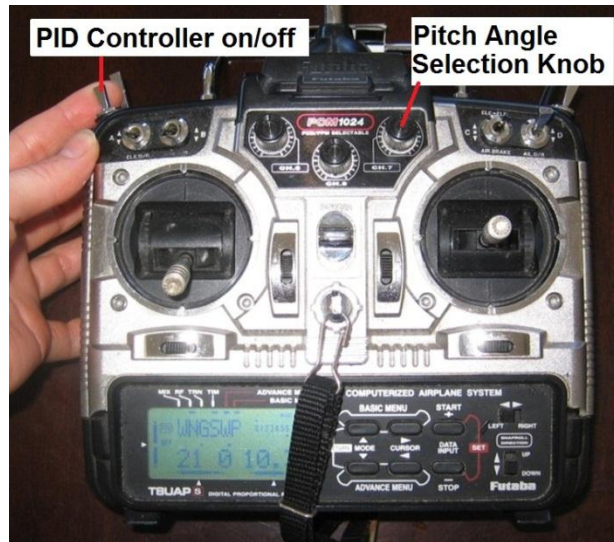
Figure 6.7: The RC transmitter set up for PID control.

When the controller was off, the arduino held the wing sweep servo at the neutral sweep position. Once the pilot activated PID control, no elevator input was used: the aircraft would attempt to settle at the pitch angle specified by the knob using wing sweep as its only pitch input. Meanwhile, the arduino would record pitch angle, wing sweep angle, and elevator position to the microSD card. Flipping the controller switch off would stop data recording and halt PID control; the wings would return to neutral sweep position automatically.

Data output from the PID control mode was in the form of a text file with five data sets for each test performed:

- One value representing test start time (described as milliseconds passed from aircraft power on)
- A column of PWM values for the wing sweep servo

- A column of PWM values for the elevator servo

- A column for values corresponding to the pitch angle reading from the IMU

- A column of PWM values corresponding to the commanded pitch angle

This data could then be exported into Excel or MATLAB for plotting. Once the data was plotted, the aircraft response to manually actuated or PID-controlled wing sweep could be identified.

Chapter 7

Flight Testing

Flight testing was performed three times, with each event consisting of several tests and landings. The first flight test was the first flight of the aircraft, and was used to observe the aircraft's flight qualities. It did not focus on data collection. The second flight test used manual wing sweep control, and the arduino system was used for data collection. The last flight test used the arduino's PID controller mode, and was the final flight test of the project.

During the first flight (see Figure 7.1), the aircraft was successfully hand launched and landed on a grass field. Ailerons, elevator, rudder, and throttle operated as predicted, providing ample control. The aircraft was easily moved by wind gusts, as expected for a small RC airplane. Overall, its flight qualities with the wings in the neutral sweep position were comparable to hobby RC aircraft of similar scale.

Figure 7.1: Aircraft flying with wings in neutral sweep position.

7.1   Manual Wing Sweep Flight Testing

The second flight test was used to observe the aircraft's pitch response to wing sweep, and used the arduino's manual wing sweep mode to collect data during flight. Pitch response to wing sweep was observed, and the data collected was used during the PID controller design process.

7.1.1   Procedure

Three identical flight batteries were available, with each expected to provide 4 minutes of flight time. Therefore, the aircraft would have to be landed and powered off in order to swap batteries, and an efficient and expedient testing procedure defined in order to use the limited battery life effectively. A step by step process was defined to minimize the chance of mistakes leading to injury, aircraft damage, or data loss. This process was summarized in several checklists, which were used during both the manual wing sweep control tests and the PID control tests (checklists provided in Appendix). At least three people were required to perform a flight test: the pilot, the runner, and someone to operate the stopwatch and video camera. The general procedure for performing a manual wing sweep flight test was:

1) Position group on field for clear view of field, and to allow runner to launch airplane into the wind.

2) With the airplane and transmitter off, perform final check for any loose connections. This includes checking that the microSD card is in place.

3) Turn the transmitter on, check that throttle is off.

4) Start video camera.

5) Place the airplane on a flat surface, and use a bubble level to level the airplane. Hold level, then turn on the airplane. Count to 30 for IMU to calibrate.

6) With the airplane level, turn the arduino on and off to record to level pitch reading.

7) Pilot performs a quick control check of flight surfaces and throttle.

8) Position for running hand launch.

9) Prepare to start stopwatch at throttle up.

10) Runner holds plane level while running into the wind. Pilot applies full throttle. When runner feels plane lift, toss gently for takeoff (see Figure 7.2).

11) Pilot trims aircraft.

12) Once airplane trimmed, perform wing sweep tests

    a.   Position plane level

b. Turn arduino on, no elevator allowed while arduino on

c. Turn knob to specified sweep value and allow plane to respond

d. Arduino off

e. Return wings to neutral sweep position

f. Recover and reposition for next test

13) When stopwatch reads 3.5 minutes, plane is landed for battery swap. Entire procedure repeated.

Figure 7.2: Hand launching airplane.

Each time a wing sweep test was performed, a note was made regarding the test number, the knob position used, and any additional observations. Once testing was complete, the data from the microSD card was downloaded and exported into Excel and MATLAB for plotting.

7.1.2 Results

Pitch response due to wing sweep was observed during the manual flight testing phase, and supporting data was obtained. Forward wing sweep caused the aircraft to pitch up (see Figure 7.3), as predicted by the AVL computational model. Pitch response was strong, even at intermediate values of wing sweep: one test even led to an unanticipated loop. Because forward wing sweep caused such a strong pitch up response, backward wing sweep was not tested for fear of causing a nosedive. Instead, varied degrees of

forward wing sweep were tested. Furthermore, forward wing sweep was of more relevance to the perching problem.

Figure 7.3: Aircraft pitching up with forward wing sweep

Each test was initialized at a level (or near level) pitch angle, and elevator use was avoided during wing sweep testing. Graph 7.1 shows a sample data set obtained during the manual wing sweep testing: approximately 8° of forward wing sweep was commanded, resulting in a pitch up from level to nearly 50 degrees nose up. The dashed red line represents the time at which the wings reached their forward swept position (as shown on the top plot), and the dashed green line represents the time at which the wings were commanded back to neutral. During the time between these dashed lines, a constant pitch up was noted (middle plot), although the elevator was not being used (as proven by the bottom plot).

Graph 7.1: Flight test data from manual wing sweep test.
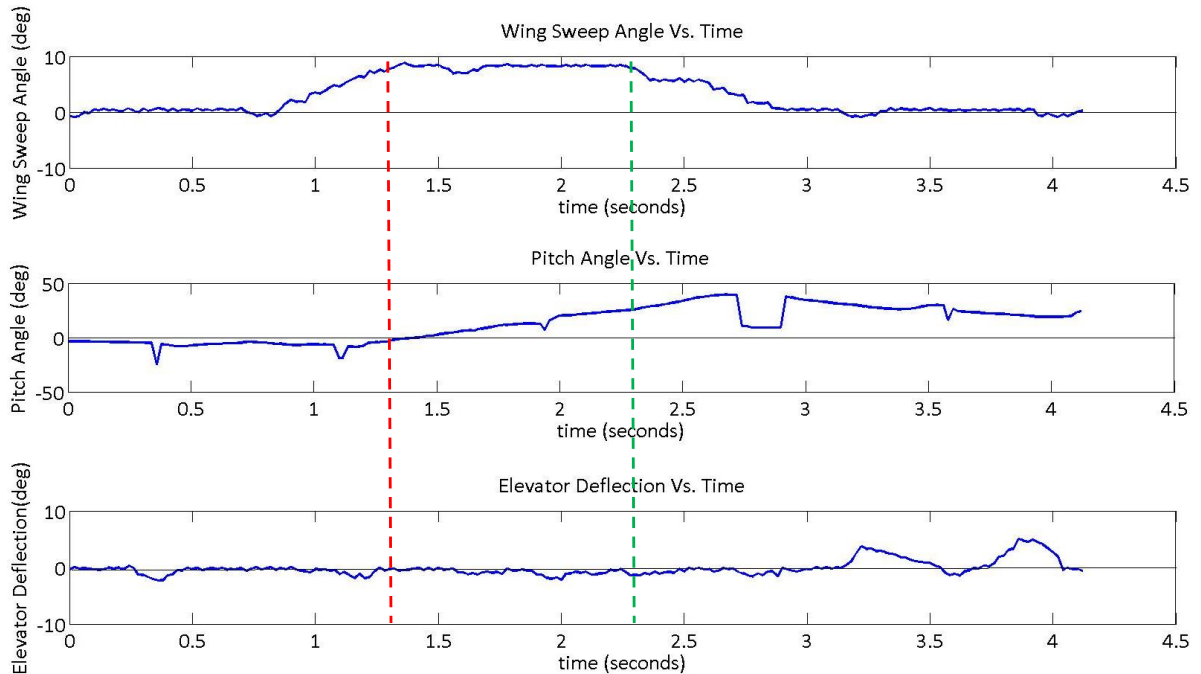
At the conclusion of one of the manual flight tests, a gust of wind caught the aircraft moments before touching down, resulting in a tail strike. The tail boom fractured at the joint, and snapped off as designed without damage to the fuselage of tail surfaces. The aircraft was repaired on the field using CA glue: glue was applied to the joint, and held for a few seconds to allow it to dry. The battery was then swapped, and the aircraft was back in the air within 10 minutes.

7.2   PID Controller Flight Testing

The PID controller flight test was intended to make a first attempt at using a simple PID controller to intelligently control pitch angle using wing sweep as the control input. One PID controller flight test was performed, using the controller described in chapter 6. The controller was able to successfully use wing sweep to adjust pitch angle, and settle at the commanded pitch angle.

7.2.1   Procedure

The procedure for the PID controller test was identical to the procedure for performing the manual wing sweep test, except the switch and knob on the RC transmitter (previously used to start data recording and select wing sweep angle, respectively) now served different functions. The switch was used to turn the PID controller on/off, and the knob used to select the goal pitch angle. In addition, flipping the switch off would automatically return the wings to the neutral position.

When the controller was turned on, it was desired that the plane be given ample time for settling at its goal pitch angle. This required extra effort to turn on the controller with the airplane at the extreme end of the field, allowing it to overfly the field while the controller was on.

7.2.2   Results

Some of the PID controller tests were cut short due to wind gusts or incorrect position on the field. During these cases, the controller did not have adequate time to settle at its goal pitch angle. However, data was obtained in which the controller was able to settle, with some steady state error (see Graph 7.2). The

top plot represents pitch angle, with the green line indicating the goal pitch angle and the blue line representing the actual pitch angle. The controller is observed to overshoot the goal (at t=6 seconds), but then settle at the goal pitch angle (near t=12 seconds). Some steady state error is observed near t=12 seconds, prior to the controller being switch off for repositioning of the aircraft.

Graph 7.2: Flight test data from PID control test.
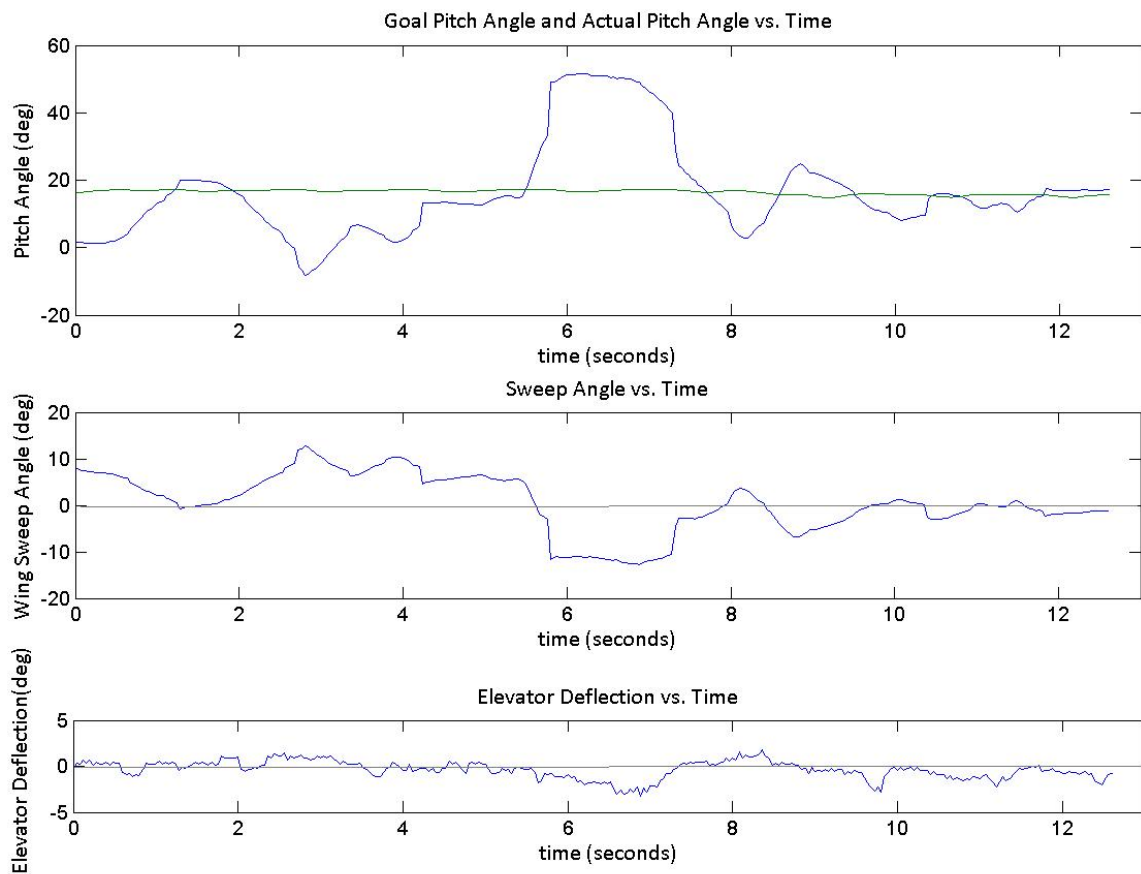
The PID controller demonstrated that it was capable of reaching the goal pitch angle, but required a long settling time with the potential for significant overshoot. Further tuning of the controller would have likely improved the controller performance, but this opportunity never occurred: flight testing came to an abrupt and unfortunate end when the plane entered a nosedive and crashed. Post-flight analysis concluded this was due to user error: the controller was switched on when the aircraft was at a high pitch angle

(almost 45°). This was much higher than expected, and the controller was not designed to handle this situation. It responded by sweeping the wings abruptly back, lowering the nose quickly. The plane responded faster than the controller could react, and the controller could not move the wings forward in time to recover. The elevator was not strong enough to fight the pitch response caused by the backward wing sweep, and the wings did not return to neutral before the plane hit the ground.

The aircraft nose was significantly damaged from the crash, and the tail boom snapped (see Figure 7.4). The central fuselage section and the wings were unharmed. All electronics survived the crash, including the microSD card. The plane was not beyond repair, but the time required to repair the airplane would not be insignificant. The aircraft had successfully demonstrated the intelligent use of wing sweep for pitch control, and the required data had been recovered. Therefore, the damaged aircraft was set aside, and the project was wrapped up.

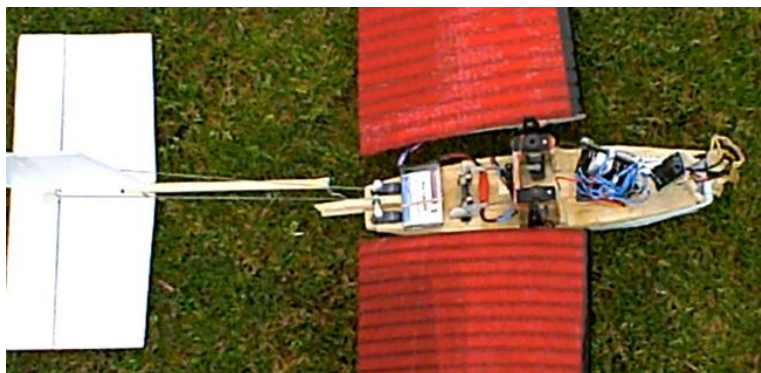**Figure 7.4:** Damaged aircraft.

After the project was complete and time was available, the aircraft was repaired to allow it to be used for demonstration purposes. The nose was rebuilt using balsa wood and fiberglass, and the tail boom glued together with CA and two supporting strips of balsa wood. The motor was reinstalled on the new nose structure, and the arduino system re-mounted in the nose.

Chapter 8

Concluding Remarks

8.1 Project Summary

Although the final flight test ended with a damaged aircraft, the desired data was obtained from the tests performed. Wing sweep was observed to cause a pitch response, thus validating the concept of using wing sweep for pitch control. Furthermore, a PID controller was designed to successfully demonstrate closed-loop pitch control using sweep variation.

Wing sweep was observed to cause strong pitch response, thus meriting the study of wing sweep for pitch control during demanding situations requiring significant pitch response (such as perching). However, this strong response can be dangerous to the aircraft if not kept under control, as noted by the unexpected loop due to forward wing sweep and the unfortunate crash due to backward wing sweep. Therefore, it is recommended that any further attempts at using wing sweep for pitch control should incorporate additional systems to help tame this strong response, including higher sampling resolution and additional fail-safe algorithms.

8.2 Discussion

8.2.1 Other Ideas

This project looked at a novel method of pitch control, inspired by the avian perching problem. Wing sweep was proven to be an effective method for pitch control in cruising flight, but it's effectiveness during other flight conditions (such as perching) is still unknown and would be purely speculation. Further research would be required to fully understand its potential for pitch control during perching.

The idea of using wing sweep for pitch control was selected as a biomimetic technique, but there are other methods which would theoretically cause similar pitching effect. Sweeping the wings simply moves the center of lift around, changing the moment arm between the center of lift and the center of

gravity. Changing the length of this moment arm causes a change in pitching moment, and a pitch response results. Consider the following simple equation:

$$M = Fd \qquad (8.1)$$

This familiar equation simply states that a moment is caused by a force (F) applied at a moment arm (d). Wing sweep variation altered 'd' by changing the position where the lift force acted. Using the same equation, consider the following possibilities:

- Change 'd' by moving center of gravity: moving the battery mass in flight would provide a center of gravity change.

- Change 'F' by changing wing properties: varying the camber of the wing would change the amount of lift produced.

- Change 'd' by sweeping wings, but consider moving battery mass at the same time to 'cancel out' the center of gravity change caused by moving the wings.

The suggestions listed above would all be interesting points to consider when researching novel pitch control methods for a small UAV. The use of an elevator (in either standard configuration or as a canard) is a well-understood and reliable pitch control method for most flight conditions. It works simply by keeping 'd' constant while varying 'F' in (8.1). The simple idea conveyed by (8.1) is a core concept when considering aircraft stability and control, and is the reason all standard aircraft control surfaces (elevator, rudder, aileron) work. These familiar surfaces simply keep 'd' constant while varying 'F'.

What makes a novel method like varying wing sweep preferable over conventional methods such as elevator deflection? It will depend on the flight condition and the particular constraints of the problem. If an aircraft cannot have an elevator for some reason, then wing sweep may be useful for pitch control in cruising flight. Otherwise, it will add a level of complexity that is probably unnecessary for standard aircraft in which an elevator can be employed.

8.2.2   Another Look at Perching

After displaying its effectiveness in simple cruising flight, the most application for wing sweep pitch control may be found in high angle of attack, stalled flight. This was the motivation for the project, and wing sweep was never expected to be a replacement for elevator-actuated pitch control during cruising flight. Experimenting with wing sweep in this more familiar flight regime simply providing a first step towards the more advanced perching problem. Now that wing sweep has proven effective in this simpler scenario, it can be reconsidered for the more advanced perching problem.

The flow around an aircraft in stalled, high angle of attack flight is complex and difficult to model. To take a first look at this complex problem, consider the simplest model possible: consider a stalled airplane falling towards a target with its wings and elevator simplified as flat plates (see Figure 8.1.) The flat plates cause drag forces as they move through the air, represented as forces F_W and F_D. Each force acts at a distance from the center of gravity (D_W and D_T for the wing a tail respectively), thus creating moments about the center of gravity of the falling airplane (M_W and M_T for the wings and tail respectively). The plane at the top of Figure 8.1 has its wings in a neutral sweep position, causing the force F_W to act behind the center of gravity. In this case, both the wing and the tail are causing moments in the same direction, leading to a nose down tendency. The plane at the bottom of Figure 8.1 has its wings swept forward: the force F_W now acts in front of the center of gravity. The moment M_W created by the wing is now in the opposite direction as the moment created by the tail M_T. By varying D_W, the magnitude of M_W can be varied to be less than, equal to, or greater than magnitude M_T. The relative magnitudes of M_W and M_T dictate the aircraft pitching properties caused by the flat plate drag. The magnitudes of F_W and F_T will determine the speed at which the aircraft descends toward its target.
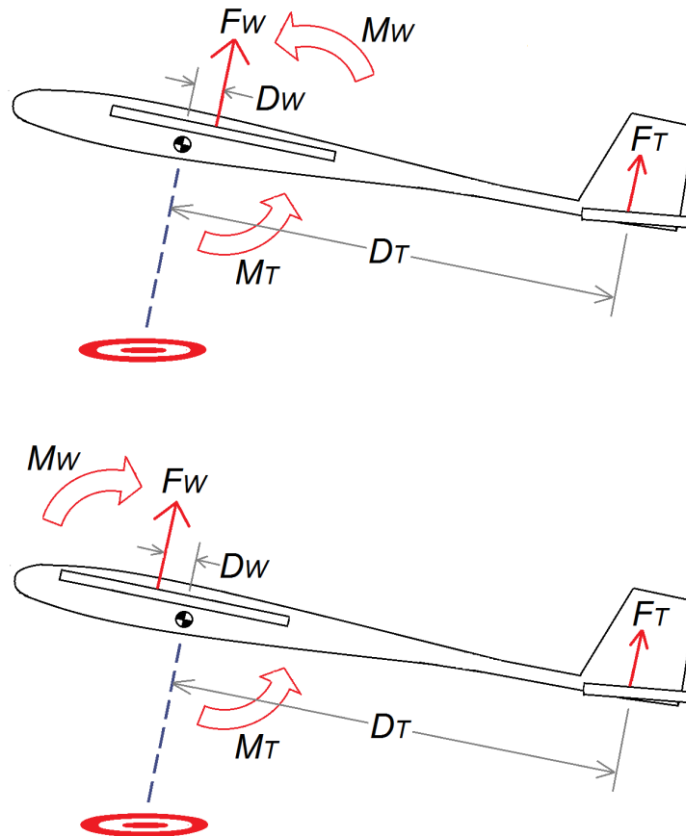
Figure 8.1: Falling airplane with flat plate surfaces

The simplified concept shown in Figure 8.1 assumes that the center of gravity has not changed as the wings are swept forward: this will not be true in a real life scenario. The center of gravity will move forward with the wings, the key is making sure that the center of force for the falling wing can move in front of the center of gravity. During cruising flight, this would be akin to moving the neutral point in front of the center of gravity, leading to a negative static margin and negative longitudinal static stability. The aircraft used for this project retained positive static margin, thus retaining positive longitudinal static stability even with the wings swept fully forward. Therefore, the experimental aircraft used for this project would not be an ideal model for experimenting at high AOA. An aircraft with lighter wings relative to the body mass could permit this condition, allowing for study at high AOA. However, this would provide the capability to generate negative longitudinal static stability, requiring more control effort.

Looking again at Figure 8.1, another potential control method can be visualized: changing the distance between the tail and the center of gravity (D_T). Nature does not employ such a method, but an extendable tail boom could allow aircraft to change this parameter. This idea, along with the other perturbations discussed in section 8.2.1, could be used along with (or in the place of) wing sweep to provide pitch control at high AOA.

8.3   Recommendations

The results from this project suggest that avian-inspired flight techniques can be successfully applied to small UAVS, and future research into the biomimetic perching problem would be valuable. However, this problem must be approached with patience and caution: even a small sub-problem proved to be a tricky and time-consuming pursuit. The seemingly effortless maneuvers accomplished by birds are undoubtedly dictated by complex flow control which we have only begun to understand.

It is recommended that more sophisticated CFD software be used for any future research into the perching problem: AVL is limited to low angles of attack, and is not intended to model turbulent, complex flow (such as may occur around a flapping bird wing). More advanced CFD analysis could potentially be used to improve the controller design process by providing a more reliable system model.

The construction process for this project relied upon tedious and careful craftsmanship. Although the final product performed well, some flaws were inevitably introduced into the aircraft as a result of the hand construction techniques. The use of milling machines and other computer-controlled equipment is highly recommended to minimize such errors for future aircraft.

Higher data sampling rates and faster onboard processing would have improved the controller's ability to respond to wing sweep changes. Faster and more powerful microcontrollers are recommended for future aircraft, especially if more degrees of control freedom are required. Furthermore, the aircraft used in this project relied upon an IMU as its only sensor input. Additional sensors (for measuring AOA, airspeed, wing position, etc.) would have been valuable additions. However, weight restrictions would not permit the inclusion of such sensors, even if they could be acquired for such a small aircraft. It is recommended that if at all possible, future aircraft include these devices.   However,   never   underestimate   the   significance   of

adding weight to a small UAV: half an ounce may not sound like much, but can negatively impact wing loading. Obsessive tracking of aircraft weight and balance will help make sure the aircraft flies as desired.

Finally, never be discouraged by a crash. In the words of aerospace legend Burt Rutan: "testing leads to failure, and failure leads to understanding". Consider each failure a new learning opportunity, and move on. Perhaps the most valuable piece of advice for those considering experimenting with RC aircraft: always keep a bottle of CA glue with you on the field. It could very well make a bad day good again.

Bibliography

[Abdulrahim 04]   Abdulrahim, Mujahid. *Dynamic Characteristics of Morphing Micro Air Vehicles*. Thesis. University of Florida, 2004. Print.

[Aerovironment]   *AeroVironment, Inc. (AV) : Unmanned Aircraft Systems, Electric Vehicle Charging Systems, Power Cycling & Test Systems*. Web. 1 May 2011. <http://www.avinc.com/>.

[AMA]   *Academy of Model Aeronautics*. Web. <http://www.modelaircraft.org/>.

[Anderson 01]   Anderson, John David. *Fundamentals of Aerodynamics*. 3rd ed. New York: McGraw-Hill, 2001. Print.

[Denewiler 11]   Denewiler, Thomas. *Robot Traffic School: Improving Autonomous Navigation in EOD Robots*. Thesis. University of California San Diego, 2011. Print.

[Desbiens]   Desbiens, Alexis L. *Perching Project*. Web. <http://bdml.stanford.edu/twiki/bin/view/Main/PerchingProject>.

[DiStefano 95]   DiStefano, Joseph J., Allen R. Stubberud, and Ivan J. Williams. *Schaum's Outline of Theory and Problems of Feedback and Control Systems*. New York: McGraw-Hill, 1995. Print.

[DIY Drones]   *DIY Drones*. Web. <http://diydrones.com/>.

[Dorf 05]   Dorf, Richard C., and Robert H. Bishop. *Modern Control Systems*. Upper Saddle River, NJ: Pearson Prentice Hall, 2005. Print.

[Drela]   Drela, Mark. *AVL*. Web. <http://web.mit.edu/drela/Public/web/avl/>.

[Goldner]   Goldner, Jerry. *Profiles of Nature Wildlife Photography*. Web. <www.profilesofnature.com>.

[Getty Images]   *Getty Image: Stock Photography*. Web. <www.gettyimages.com>

[Hayes 99]   Hayes, M. H. *Schaum's Outline of Theory and Problems of Digital Signal Processing*. New York: McGraw Hill, 1999. Print.

[Hitec]   *HS-5085MG Premium metal gear micro servo*. Web. <http://www.hitecrcd.com/products/digital/digital-micro-mini/hs-5085mg.html>

[Hoburg 09]   Hoburg, Warren. "System Identification of Post Stall Aerodynamics for UAV Perching." *American Institute of Aeronautics and Astronautics* (2009). Web. <http://groups.csail.mit.edu/robotics-center/public_papers/Hoburg09a.pdf>.

[ImageJ]   "ImageJ." *RSB Home Page*. Web.. <http://rsbweb.nih.gov/ij/>.

[Kaw 06]   Kaw, Autar K. *Mechanics of Composite Materials*. Boca Raton, FL: Taylor & Francis, 2006. Print.

[Langewiesche 72]   Langewiesche, Wolfgang, and Leighton Holden Collins. *Stick and Rudder: an Explanation of the Art of Flying*. New York: McGraw-Hill, 1972. Print.

[Liu 04]   Liu, Tianshu, K. Kuykendoll, R. Rhew, and Steven Jones. "Avian Wings." Proc. of 24th AIAA Aerodynamic Measurement Technology and Ground Testing Conference, Portland. Hampton: American Institute of Aeronautics and Astronautics, 2004. Print.

[Meyers]   Meyers, Martin. *SierraBirdbum*. Web. 1 May 2011. <http://sierrabirdbum.com>.

[Moore 09]   Moore, Joseph, and Russ Tedrake. "Powerline Perching with a Fixed-Wing UAV." *American Institute of Aeronautics and Astronautics* (2009). Web. <http://groups.csail.mit.edu/robotics-center/public_papers/Moore09.pdf>.

[Reg Heath]   *Reg Heath's Modelflight, for Model Flight Enthusiasts of All Disciplines*. Web. <http://www.modelflight.regheath.com/>.

[Roberts 09]   Roberts, John, and Russ Tedrake. *On the Controllability of Fixed-Wing Perching*. Tech. Cambridge: MIT, 2009. Print.

[Tedrake 09]   Tedrake, Russ, Zack Jackowski, Rick Cory, John W. Roberts, and Warren Hoburg. *Learning to Fly Like a Bird*. Tech. Cambridge: MIT, 2009. Print.

[West Systems]   *Epoxy Chemistry.* Web. <http://www.westsystem.com/ss/epoxy-chemistry/>

[Yechout 03]   Yechout, Thomas R., and Steven L. Morris. *Introduction to Aircraft Flight Mechanics: Performance, Static Stability, Dynamic Stability, and Classical Feedback Control*. Reston: American Institute of Aeronautics and Astronautics, 2003. Print.

Appendix

Startup / Battery Swap Checklist:
1)   Position for wind and view of low pass
2)   Airplane off, Tx off
3)   Swap batteries
4)   Download data, erase SD card
5)   Note stopwatch time, reset stopwatch
6)   Reinstall and tape SD card
7)   Visual inspection of connections/aircraft
8)   Secure canopy
9)   Put aircraft on tripod
10)   Transmitter on
11)   Verify throttle off, arduino off, wings neutral
12)   Video camera on, recording start
13)   Level aircraft and hold level.
14)   Aircraft on (hold to level IMU)
15)   Arduino on and off (store level pitch reading)
16)   Check wind, position for launch
17)   Stopwatch on at throttle up

Before Going to Field
1)   Batteries at full charge
2)   Correct code loaded
3)   Arduino/IMU/SD card pins secure
4)   Servo pin correct selection, secure
5)   SD card emptied and taped
6)   Wing connections secure
7)   Aileron servo connections secure
8)   Bottom skid panel installed
9)   Video camera charged and ready

Equipment to take to field:
1)   Laptop with good battery
2)   Micro SD card adapter
3)   Tripod to level plane
4)   Bubble level
5)   Extra batteries (charged)
6)   Stopwatch
7)   Video camera (charged)
8)   Note paper
9)   CA
10)   Double sided tape
11)   Flexible tape
12)   Flight test cards